FINAL TECHNICAL REPORT

PRELIMINARY SEASAT–A SCATTEROMETER ANTENNA DESIGN

EES/GIT Project A–1617–010

By

D. G. Bodnar, N. T. Alexander,
and R. R. Sheppard

Prepared for

APPLIED PHYSICS LABORATORY
THE JOHNS HOPKINS UNIVERSITY
Silver Spring, Maryland 20910

Under

Prime Contract N00017–72–C–4401
and APL/JHU Subcontract 600128, TASK 5

October 1975

1975

ENGINEERING EXPERIMENT STATION
Georgia Institute of Technology
Atlanta, Georgia 30332

ENGINEERING EXPERIMENT STATION
Georgia Institute of Technology
Atlanta, Georgia 30332

PRELIMINARY SEASAT-A SCATTEROMETER ANTENNA DESIGN

Final Technical Report on

EES/GIT Project A-1617-010

By

D. G. Bodnar, N. T. Alexander, and
R. R. Sheppard

Prepared for

APPLIED PHYSICS LABORATORY
THE JOHNS HOPKINS UNIVERSITY
Silver Spring, Maryland 20910

Under

Prime Contract N00017-72-C-4401

and

APL/JHU Subcontract 600128, Task 5

October 1975

ABSTRACT

A preliminary electrical, mechanical, and thermal design for the Mode I and Mode II flight antennas of the SEASAT-A satellite scatterometer has been performed. A non-resonant edge-slot array in a trough horn provides horizontal polarization, and a separate non-resonant broadwall slot array in a similar trough horn provides vertical polarization. These antennas operate at 14.6 GHz and combine to produce a dual polarized fan beam. A stiffened thin-wall box-beam structure is used to maintain the requisite mechanical tolerances. Both mechanical and electrical design considerations of the antenna are presented. Full frequency, quarter-length brassband model antennas were fabricated for both the edge slot and broadwall slot arrays and tested for conformance to the current specifications. Measured data on these antennas is presented and indicates that the desired performance from the full length antennas can be achieved with the design utilized.

TABLE OF CONTENTS

LIST OF FIGURES

LIST OF FIGURES (continued)

LIST OF FIGURES (continued)

LIST OF TABLES

I. INTRODUCTION

A microwave scatterometer experiment is one of the microwave experiments planned for the SEASAT-A satellite. The microwave scatterometer determines wind speed and direction by measuring radar cross section of a surface element of the ocean from two orthogonal azimuth elements. The function of the scatterometer antennas is to provide the scatterometer radar with dual polarized, fan-beam views of the earth's surface. Four beams oriented at $\pm 45°$ and $\pm 135°$ from the velocity vector are needed and will be produced by the Mode I antennas. A fifth beam oriented along the velocity vector is also required and will be produced by a Mode II antenna. The beam centers lie along a cone with a half-angle of 40.7° from nadir. These five fan beams will be produced by five waveguide antennas properly oriented to produce the correct footprint on the earth. One design is used for the Mode I antennas and a slightly modified design is used for the Mode II beam. The desired footprint of the beams on the earth's surface is obtained by deployment of the antennas through single axis rotation from the spacecraft vehicle.

The Engineering Experiment Station at the Georgia Institute of Technology has performed a preliminary electrical, mechanical, and thermal design for the Mode I and Mode II scatterometer flight antennas. This report documents the design studies and presents the final results and recommendations resulting from the study. In addition, this report presents measured data on full frequency, quarter-length models of the scatterometer antennas which were designed and built to validate the electrical performance predicted by the study.

Inquiries concerning the contents of this report should reference Project A-1617-010 and should be directed to:

Director, Systems and Techniques Laboratory
Engineering Experiment Station
Georgia Institute of Technology
Atlanta, Georgia 30332.

II. FLIGHT ANTENNA DESIGN

A. Performance Requirements

The electrical performance requirements for the scatterometer antenna of the SEASAT-A satellite are given in Table I. These requirements differ from those of a previous SEASAT-A antenna study [1] primarily in that the frequency was changed from 13.9 GHz to 14.6 GHz and that the sidelobe requirements have been relaxed. The mechanical performance requirements for this antenna are given in Table II and Figures 1, 2, 3. A preliminary electrical, mechanical and thermal design for the scatterometer antenna has been performed based on the new requirements. The results of this design are presented in this report.

B. Electrical Design

Five dual-polarized fan beams are required from the SEASAT-A scatterometer antenna system. The four beams of the Mode I antenna are identical in all respects except for their angular orientation in space. The Mode II antenna has the same narrow-plane beamwidth as the Mode I antenna, but its broad plane beamwidth is roughly twice that of the Mode I antennas. After considering a number of alternative antenna designs [1], an optimum antenna for the scatterometer radar was selected to be a pair of slotted waveguides feeding separate trough horns. A traveling-wave array was recommended rather than a standing-wave array in order to increase the bandwidth available from the relatively long waveguide structure. Separate slotted arrays in separate trough horns are used to obtain the desired vertical and horizontal polarizations and maintain good isolation between the two polarization channels. Horizontal polarization is obtained from an edge slot waveguide array feeding a trough horn while vertical polarization is obtained from a broadwall slot array feeding a separate trough horn.

TABLE I

MICROWAVE PERFORMANCE REQUIREMENTS FOR THE SEASAT-A SCATTEROMETER ANTENNA

Parameter	Mode I Antenna	Mode II Antenna
Frequency	14.595 GHz	14.595 GHz
Bandwidth	±1 MHz	±1 MHz
View Angles	±45° and ±135° with respect to velocity vector	Single beam along velocity vector
	40.7° with respect to nadir	42.0° with respect to nadir
3-dB Beamwidth	0.5° Az by 25° El	0.5° Az by 40° El
Power Gain	32.5 dBi peak	30 dBi peak
	25 dBi @ ±19.5° El	17 dBi @ ±42.0° El
Elevation Pattern Slope	≤1.0 dB/° over ±19.5° El	≤1.3 dB/° over ±42.0° El
Polarization	Vertical and Horizontal	Vertical and Horizontal
	Cross Pol ≤ -20 dB	Cross Pol ≤ -20 dB
Sidelobe Levels	-20 dB Az	-20 dB Az
	-12 dB El	-12 dB El
Beam Pointing Error	TBDL	TBDL
Gain Variation due to Thermal Beam Steering Predictable to Within	±0.2 dB max	±0.2 dB max
Isolation Between Vertical/Horizontal Antennas	>20 dB	>20 dB
Radiated Power	2.5 kW peak, 15W avg	2.5 kW peak, 15W avg
	125W peak, 30W avg	125W peak, 30W avg
VSWR	≤1.3:1	≤1.3:1
Weight	40 lb max (30 lb goal)	40 lb max (30 lb goal)

TABLE II

MECHANICAL PERFORMANCE REQUIREMENTS
FOR THE SEASAT-A SCATTEROMETER ANTENNAS

Envelope:	See Figure 1.	
Weight:	40 pounds each (30 pound goal)	
Quasi-static acceleration*:	Axial	Lateral
Liftoff	- 4.0g	±6.0g
Maximum dynamic head	± 2.5g	±8.0g
Maximum acceleration	+10.0g	±4.0g
Shock:		
Shape	half sine wave	
Duration	0.5 millisecond	
Amplitude	100g	
Acoustics:	See Figure 2.	
Random Vibration:	See Figure 3.	
Temperature, pressure & humidity:	Ground checkout, launch and earth orbit environments	
Reliability:	1 year operational	

*positive load factor is acting aft (forward acceleration).

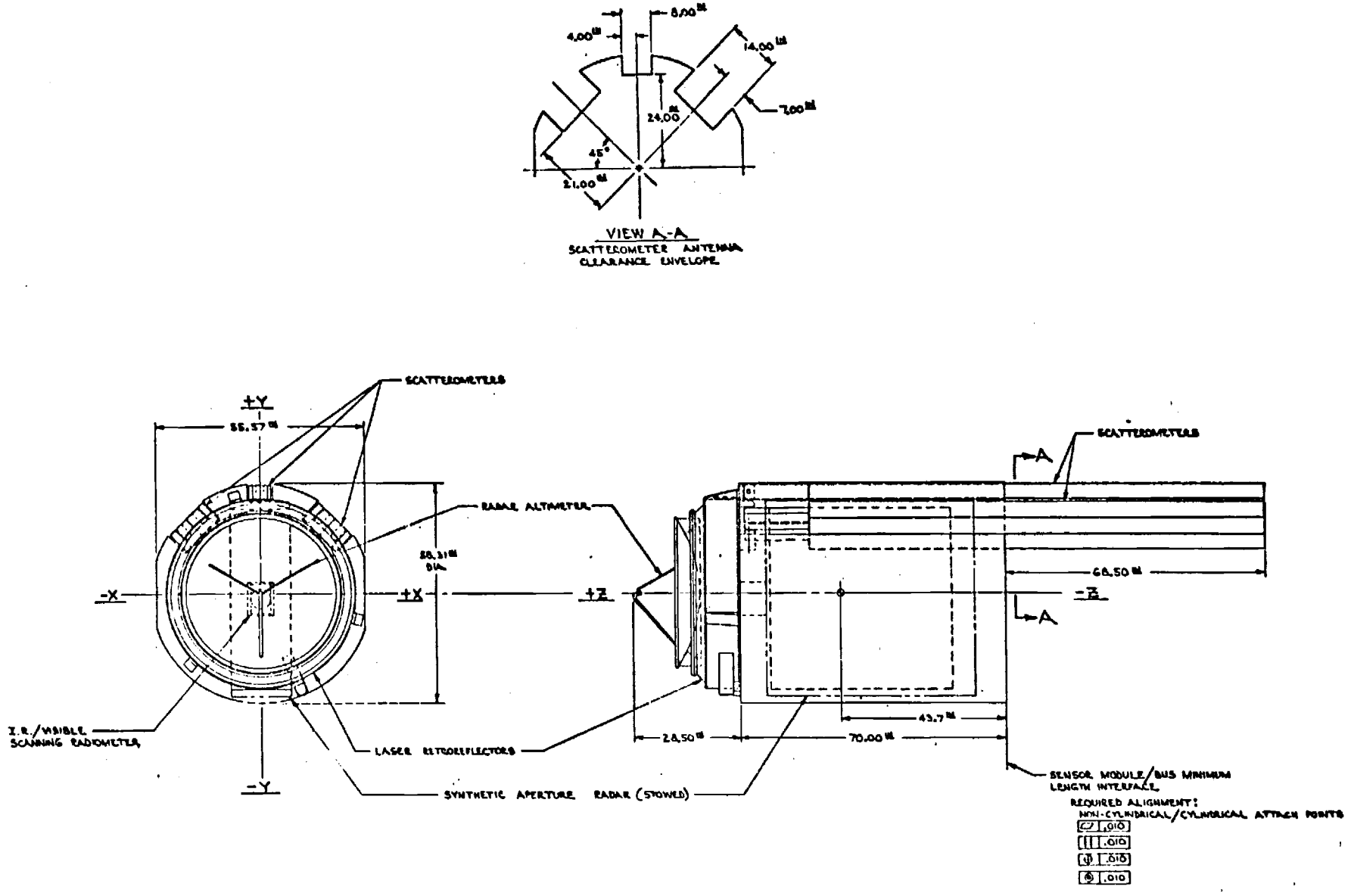

Figure 1. SEASAT launch configuration.

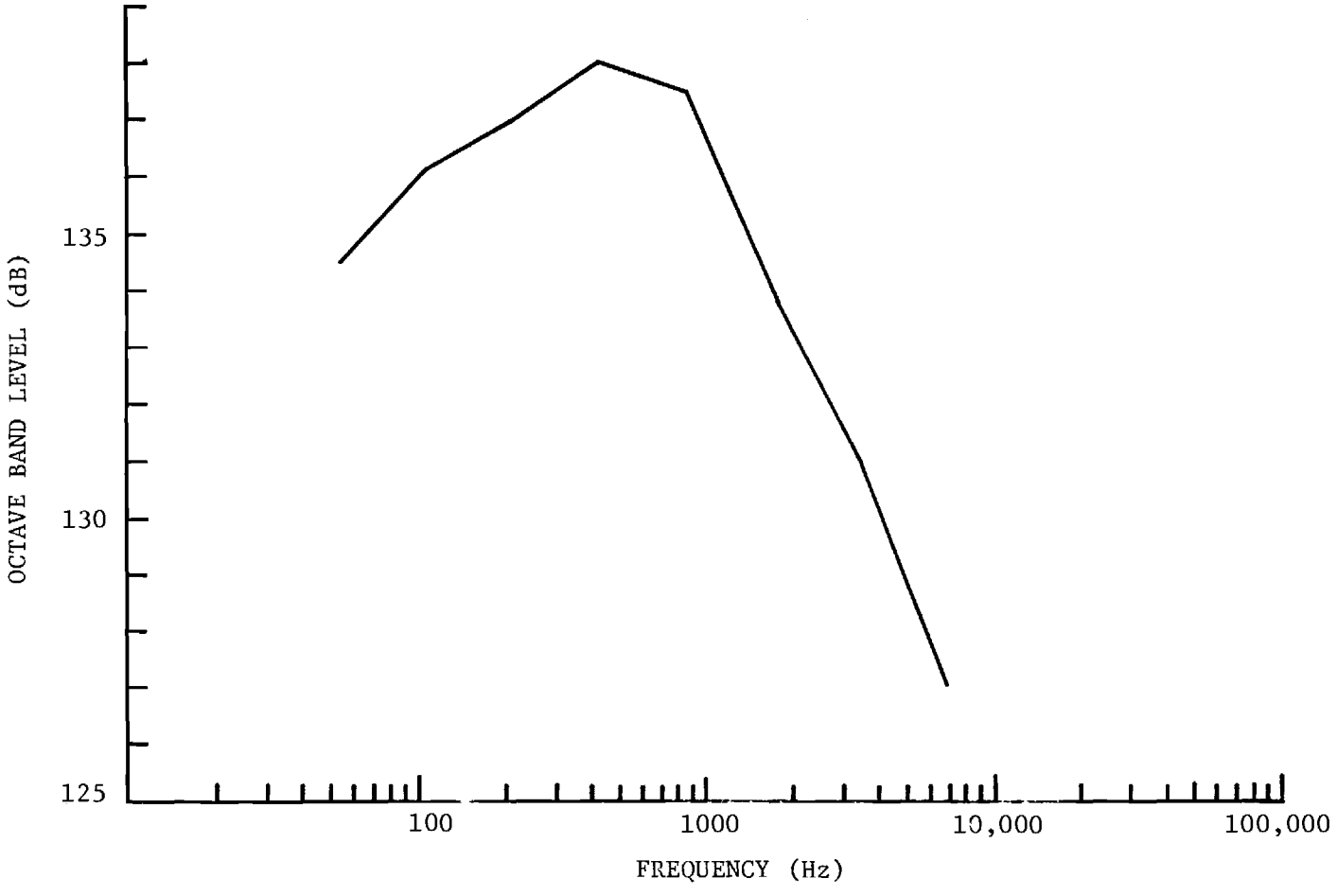

Figure 2. Acoustic noise level for the scatterometer antenna.

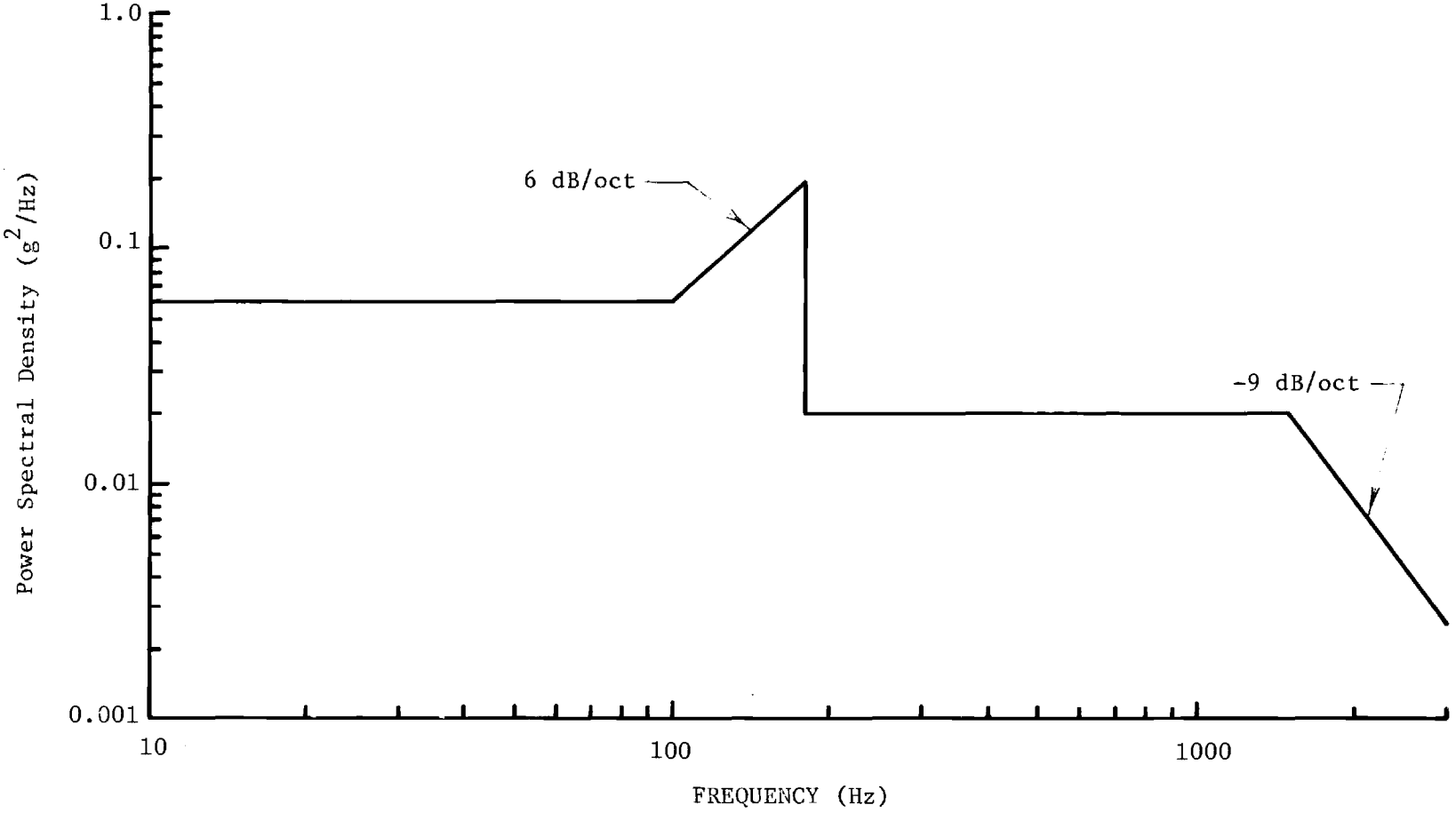

Figure 3. Random vibration spectrum for the scatterometer antenna.

1. Slot Conductance

Accurate slot data must be available on the individual slots in order to perform an accurate electrical design for a slotted waveguide antenna. To obtain this information, slot conductance measurements were performed on four broadwall slot test sections and on four edge slot test sections. Each section consisted of 20 identically displaced slots. In the broadwall case, displacements of 0.13, 0.76, 1.14 and 1.52 mm (0.005, 0.030, 0.045 and 0.060 inches) were used for the four sections with slots alternately displaced about the center line. It was felt that this range of slot displacements would cover the range of displacements encountered in the final antenna design. The four edge slot sections consisted of 5°, 10°, 15°, and 20° tilts of the slots. Slot conductance measurements were performed on all these sections using the lossy moving short technique [2]. Broadwall slot conductance measurements were made for one length of slots. The slots were then cut slightly longer, and remeasured. This process was repeated until the peak in the conductance curve had been passed. Similarly, for the edge slots, the slots were cut to a particular depth and slot conductance measurements made. The slots were then cut deeper and remeasured, and the cutting measurement process repeated until the peak of the conductance curve had been past. From these measurements the resonant length of the slots was determined as were the slot conductance versus slot displacement and versus slot angle. A design can be performed from these data to obtain a slot antenna with the desired sidelobe level in the azimuth plane. The slot conductance measurements were made in the final horn geometry which is planned for the flight antennas. In this way the slot conductance measurements were made in the actual environment that they would experience in final flight antennas.

2. Horn Design

A cross section of the basic broadwall slot antenna is shown in Figure 4. This antenna consists of a slotted waveguide feeding a parallel plate section which, in turn, is attached to a trough horn. Figure 5 shows the basic edge slot antenna configuration. This antenna also comprises a slotted waveguide, parallel plate section, and trough horn.

The height of the parallel plate section for the broadwall slot antenna was selected so that second order lobes in the E-plane pattern would not occur. The length of the parallel plate section was chosen to sufficiently attenuate any higher order modes that may be present in the parallel plate section.

The length of the horns, L_B and L_E, were chosen long enough to prevent excessive phase error in the aperture. A horn length was selected using the usual criterion that the phase error at the horn aperture be less than $\lambda/8$. For the Mode I antennas the horn aperture was selected to be 4.19 cm (1.65 inches) for the broadwall slot array horn and 5.72 cm (2.25 inches) for the edge slot array horn in order to produce the required beamwidth. The edge slot horn aperture must be bigger than that for the broadwall slot antenna due to the cosine taper of the aperture distribution for the edge slot array. The Mode II horn requires a 2.62 cm (1.03 inch) aperture for the broadwall slot antenna and a 3.35 cm (1.32 inch) aperture for the edge slot antenna.

3. Array Design

A design sidelobe level of -25 dB was chosen for the azimuth plane to provide some tolerance in achieving the desired -20 dB sidelobe level. A -25 dB Taylor distribution was used to produce the narrow dimension of the fan beam since this distribution results in the shortest length array for the desired beamwidth. Based on the above distribution, the edge slot array and the broadwall slot array will each have 166 slots spaced 1.52 cm (0.6 inches) apart; the slot spacing was chosen to scan the beam slightly off broadside,

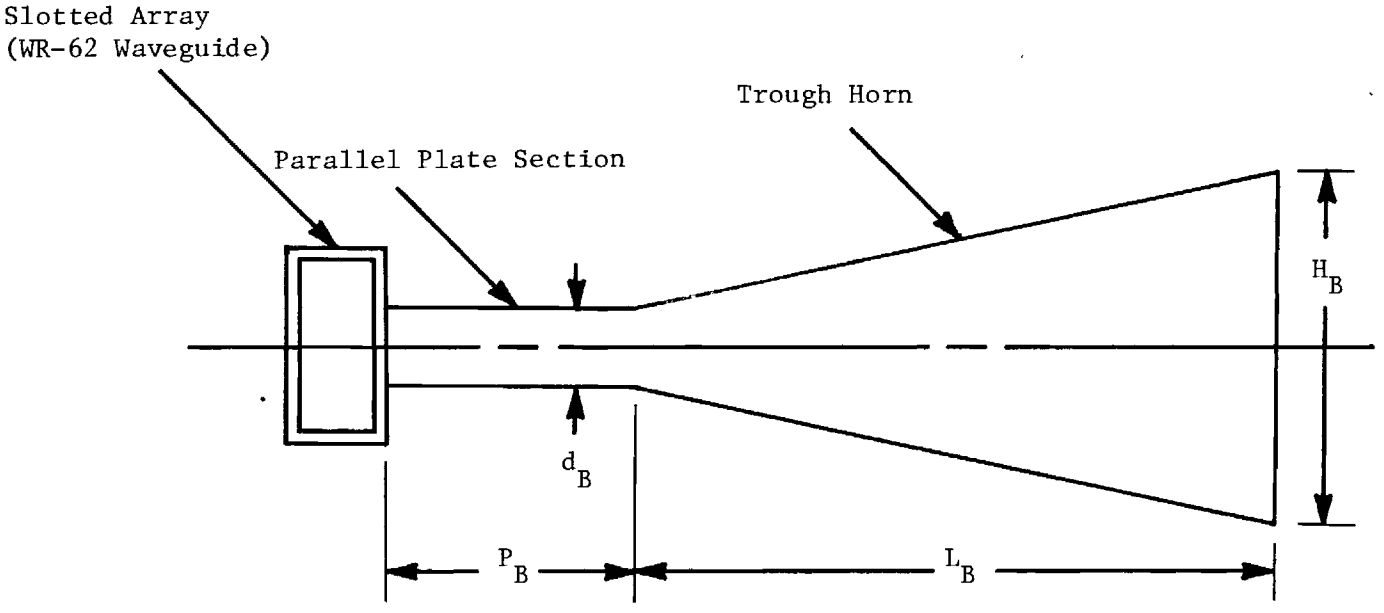

Figure 4. Broadwall slot antenna.

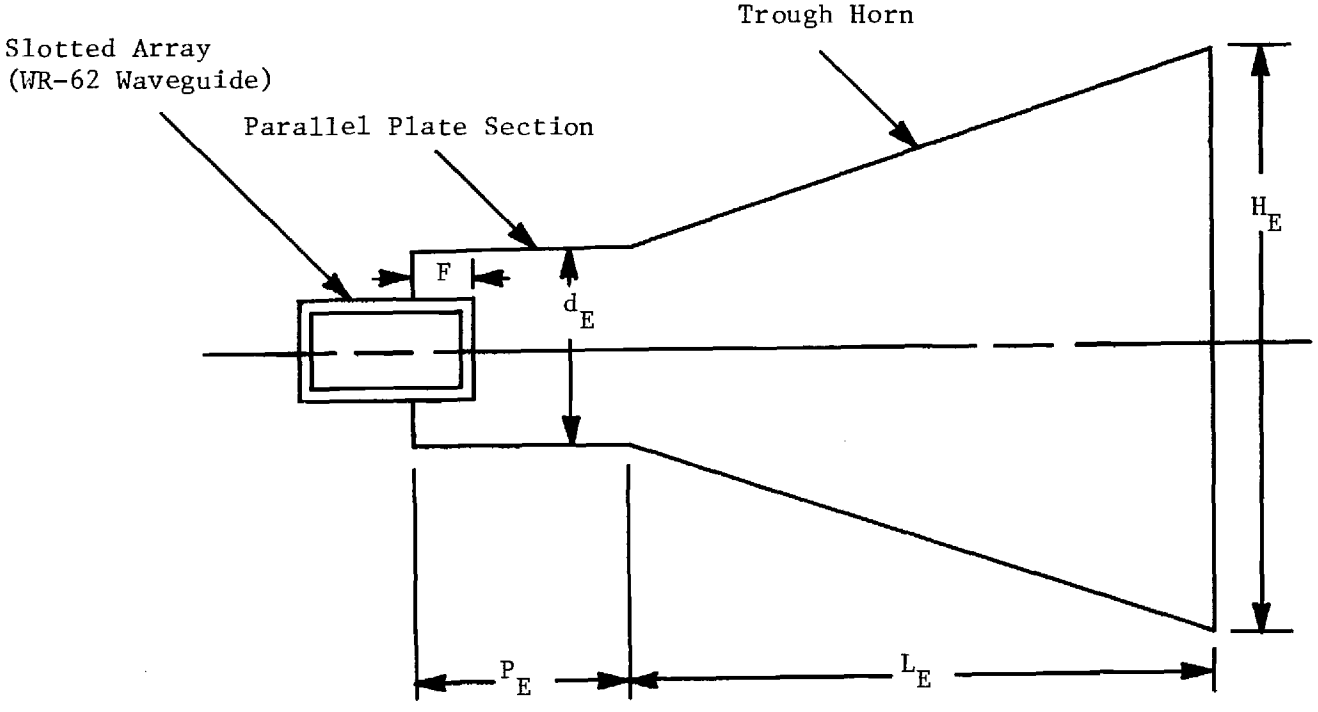

Figure 5. Edge slot antenna.

thus preventing a high VSWR condition from occurring. The 1.52 cm (0.6 in) slot spacing produces a nominal 5.0° scan of the beam from broadside toward the load end of the array. This beam scan will be removed by means of either a compensating 5° shim on the attachment flange to the antenna or by an additional 5° rotation of the antenna during deployment.

4. Tolerance Analysis

Tight mechanical tolerances must be held on the SEASAT-A scatterometer antennas since they are narrow beam, high frequency devices. Some simple calculations are instructive in assessing the effects of tolerances on main beam pointing direction.

The direction of the main beam of the array is given by

$$\theta_m = \sin^{-1}\left(\frac{\lambda_o}{\lambda_g} - \frac{\lambda_o}{2d}\right) \qquad (1)$$

where

θ_m = beam direction from broadside measured toward the load

$\lambda_o = 2\pi/f$ = free space wavelength

$\lambda_g = \lambda_o(1-(\lambda_o/2a)^2)^{1/2}$ = guide wavelength

d = slot spacing

a = guide width

T = temperature of waveguide

α = thermal coefficient of expansion of waveguide

f = frequency of operation

Performing a Taylor series expansion of θ_m in Equation 1 for the variables f, d, and a, retaining only terms through linear, and evaluating at the expected design values of

$$f_o = 14.6 \text{ GHz}$$
$$d_o = 1.52 \text{ cm} = 0.600 \text{ inches} \qquad (2)$$
$$a_o = 1.58 \text{ cm} = 0.622 \text{ inches}$$

gives

$$\theta_m = 4.9555° + 70.70° \frac{\Delta f}{f_o} + 38.74° \frac{\Delta d}{d_o} + 31.95° \frac{\Delta a}{a_o} \cdot \qquad (3)$$

Equation 3 permits deviations in beam pointing direction to be determined due to deviations in f, d, or a. Note that d and a are both functions of temperature. Changes in temperature alone change θ_m as follows

$$\theta_m = 4.9555° + 70.69°\alpha T = 4.9555° + 9.048 \times 10^{-4} \Delta T(°F) \qquad (4)$$

for aluminum waveguide.

The changes, $\Delta\theta_m$, in beam pointing direction can be evaluated from (1) through (4) for various changes in f, d, a, or T. Only one set of $\Delta\theta_m$ values need be calculated since the changes in θ_m are linear with changes in f, d, a, and T. Table III lists a representative set of variations in θ_m.

TABLE III

CHANGES IN BEAM POINTING DIRECTION DUE TO CHANGES IN FREQUENCY, MECHANICAL DIMENSIONS, AND TEMPERATURE

Parameter Change	Change in Beam Pointing Direction, $\Delta\theta_m$
$\Delta f = \pm 1$ MHz	$\pm 0.0048° = \pm 0.0097$ BW's
$\Delta d = \pm 0.001$ inches	$\pm 0.065° = \pm 0.13$ BW's
$\Delta a = \pm 0.001$ inches	$\pm 0.051° = \pm 0.10$ BW's
$\Delta T = \pm 100°F$	$\pm 0.090° = \pm 0.18$ BW's

From Table III it can be seen that for the 0.5° beamwidth scatterometer antennas:

1. The beam will be scanned by about ± 0.13 beamwidths due to expected errors in slot position of $\Delta d = \pm 0.001$ inches. Hence, the beam center cannot be predicted accurately enough and will have to be measured after construction.

2. The beam will be scanned by about ± 0.30 beamwidths due to expected errors in waveguide width of $\Delta a = \pm 0.003$ inches. Again, the beam center cannot be predicted accurately enough and will have to be measured after construction.

3. According to calculations by Georgia Tech, the exterior of the antenna will experience a -60°F to +200°F temperature change if external temperature control coatings are not used. The beam would be scanned by ± 0.23 beamwidths for the $\Delta T = \pm 130$°F if the antenna itself experiences this temperature change. Therefore, thermal coatings should be placed over the antenna to reduce the range of temperature variation that the antenna experiences. Calculations indicate that a $\Delta T = \pm 10$°F can be achieved for the entire antenna, thus reducing thermal beam shift to an insignificant level.

In addition to these fixed errors, random or systematic errors in the mechanical location of antenna aperture may occur. The major effect of these errors will be to raise sidelobe levels. To maintain -25 dB design sidelobes, the aperture must be straight and flat to within $\lambda/16$. Thus, peak-to-peak random variations in the aperture should be less than 0.13 mm (0.05 inches). Systematic bending (warping) of the aperture will also raise sidelobe levels. Representing the effect of this warping as a cubic phase error requires that the edge of the aperture be within $\lambda/16$ or 0.13 mm (0.05 inches) of a plane defined by the center of the aperture.

5. Polarizer

One technique that is available to reduce cross polarized components in the edge slot array is through the use of a polarization grid across the aperture of the horn. This technique was considered for the SEASAT-A scatterometer application. In earlier specifications [1], -25 dB cross-

polarization sidelobes were required. It was felt that a polarization grid across the horn aperture would be required to achieve these sidelobe levels from the edge slot array which has inherently high cross polarization lobes. The current requirements have relaxed the cross polarization specification to -20 dB and it is felt that this cross polarization requirement can be met by the array itself without the use of a polarization grid. Measurements made by Georgia Tech on an array similar to that which will be flight qualified showed that cross polarization lobes of 20 dB or better can indeed be achieved in practice without the use of the grid.

6. Risk Areas

The majority of the design proposed herein utilizes proven techniques for achieving the desired electrical, mechanical, and thermal performance. In particular, the gain, beamwidth, and sidelobe levels should not be difficult to obtain. A potential problem arises in achieving the desired cross-polarized sidelobes from the edge slot array. Cross polarization occurs in the edge slot array due to tilting of the slots from vertical. The larger the slot tilts, the greater will be the cross polarization. However, since adjacent slots are inclined opposite to one another, adjacent slots tend to cancel each other's cross polarization. This cancellation is not perfect, however, since the tilt of the slots at the output end of the array, for example, is greater than that of the slots at the input end of the array. The end slots are tilted more since less power is available toward the load end and so that slots must therefore be inclined at larger angles. If the desired cross polarization cannot be obtained from the array itself, then it may be necessary to add a polarizing grid over the output aperture of the edge slot trough horn. This approach would definitely lower the level of the cross polarized lobes below the desired values.

An additional problem occurs in achieving the desired -12 dB sidelobe level in the elevation plane of the broadwall slot horn. The best performance achievable for an E-plane horn (as the trough horn of the broadwall slot array is) is -13.2 dB, and this occurs when the horn is infinitely long. The E-plane sidelobes will increase when phase error is introduced into the aperture of the horn by shortening its length. Model tests must be performed to determine whether this -12 dB sidelobe level can be achieved without requiring an excessive horn length.

The two primary sources of deformation of the flight antennas are the lift-off environment and the orbital thermal environment. The predicted response of the proposed design to these environments is well within acceptable limits. Problems are possible in the fabrication of the antennas if proper tooling is not utilized. Maintaining the required dimensional tolerances over the 254 cm (100 in) length of the antennas at assembly requires the construction of very accurate fixtures. The bends in the aluminum skin require a precise mechanical break and the enforcement of exacting controls. The riveting operation must be precisely planned and executed to avoid deformation at assembly.

C. Mechanical Design

This section describes the mechanical design effort for the SEASAT-A scatterometer antenna system; both mechanical and thermal analyses upon which the design is based are presented. The predicted mechanical performance characteristics of the antennas are described and compared with the performance requirements received from APL.

1. Design Description

Five antennas are required for the SEASAT-A scatterometer antenna system. Four are Mode I antennas and one is a smaller Mode II antenna. The Mode I antennas are to be positioned about the periphery of the sensor module

in pairs. One pair is to operate at 45° with respect to the vehicle velocity vector and the other pair at -45°. The Mode II antenna is to lie perpendicular to the satellite velocity vector in the plane of the Mode I antennas.

Each Mode I scatterometer antenna unit consists of two slotted aluminum waveguide arrays. One waveguide has numerically machined edge slots and the other utilizes broadwall slots. Each is equipped with a trough horn. As shown in Figure 6, the waveguides are fitted into aluminum extrusions to insure dimensional accuracy during launch, deployment, and operation. These extrusions have a wall thickness of 3.18 mm (0.125 inch). The remainder of the structure is to be fabricated using 0.76 mm (0.030 inch) thick aluminum sheet. The trough horns are riveted directly to the extrusions. By forming the skin sheeting as shown in Figure 6, a stiffened thin-wall box-beam structure is obtained which achieves high structural integrity with minimal weight. The skin sheeting is stiffened by internal ribs spaced at 12.7 cm (5 in) intervals along the 2.54 meter (100 in) length of the antennas.

The antennas are to be insulated using space qualified polystyrene foam. As depicted in Figure 7, the Mode I antennas are tilted at 40.5° within the dual-antenna assembly. This insures that the antennas will be inclined 40.5° from nadir when in the deployed configuration. The maximum thickness of the styrofoam insulation, due to launch configuration space limitations, is approximately 7.37 cm (2.9 in).

A cross-sectional drawing of the insulated Mode II antenna assembly appears in Figure 8. This antenna also has a 2.54 meter (100 in) inside trough length. The box-beam dimensions, however, are reduced. The same fabrication technique used in the Mode I design described above is utilized for the smaller Mode II antenna.

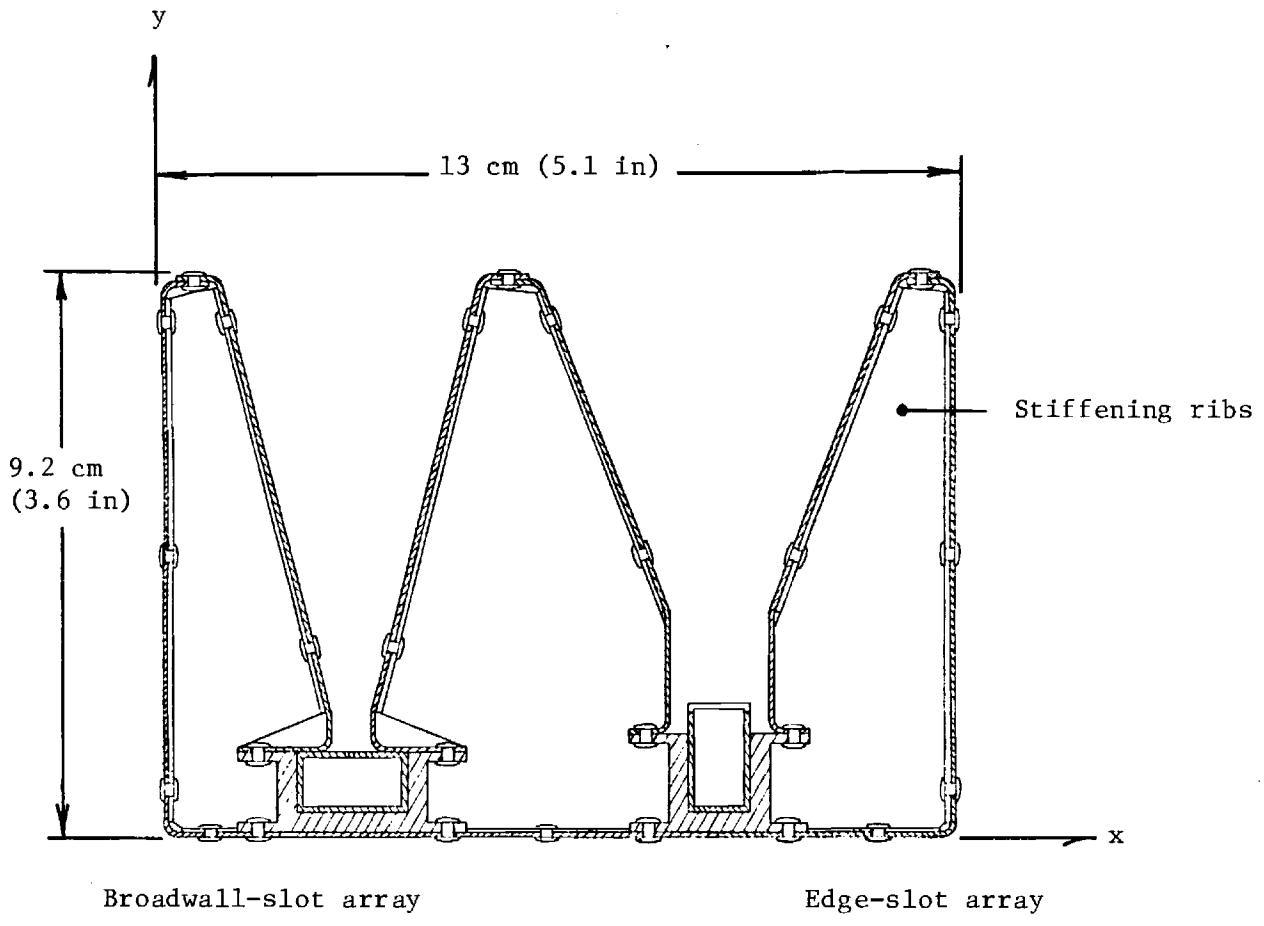

Material: 0.76 millimeter (0.030 inch) aluminum sheet
Length: 2.54 meters (100 inches)

Figure 6. Mode I scatterometer antenna cross section.

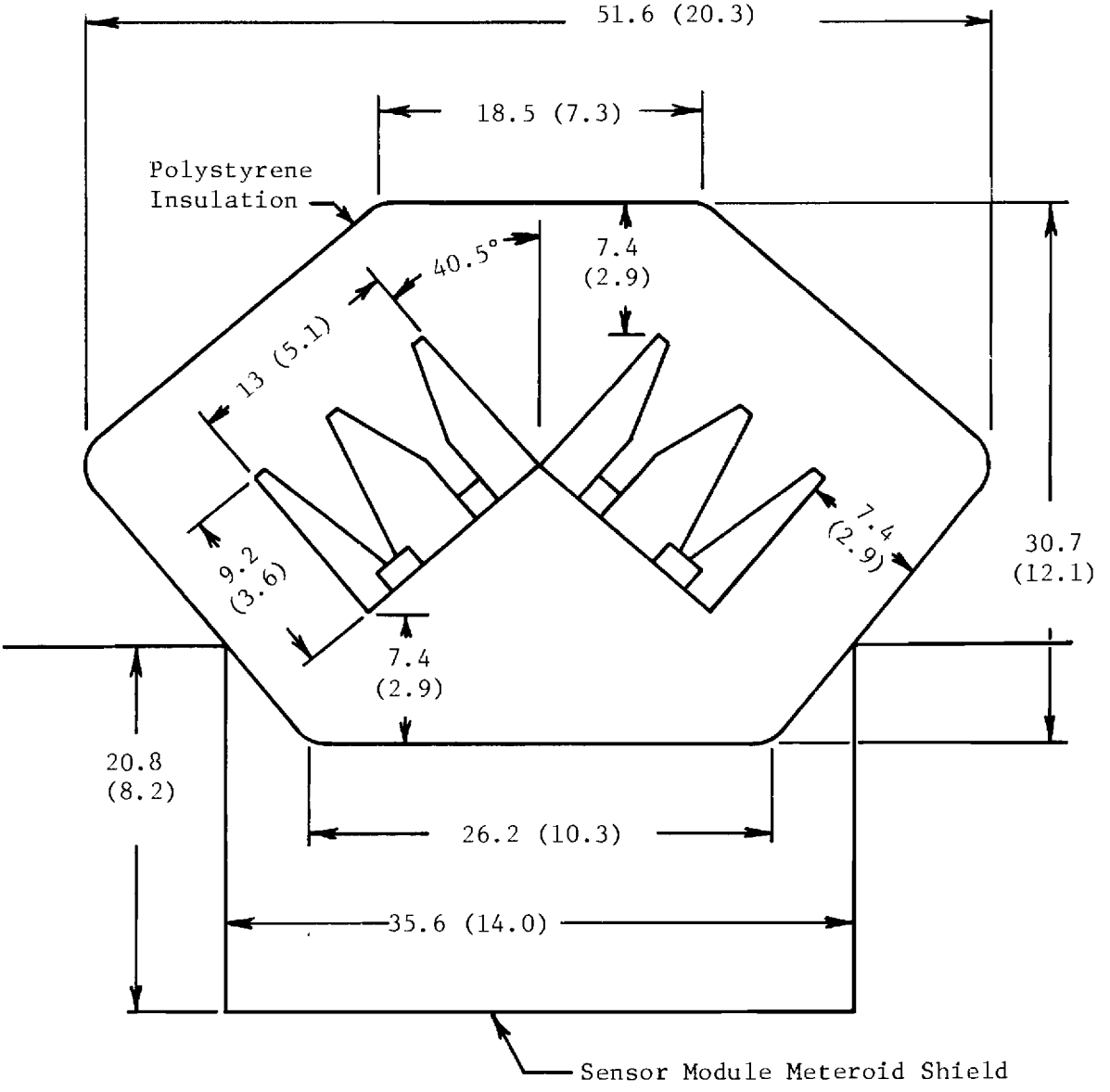

Dimensions: Centimeters (inches)

Figure 7. Insulated Mode I dual antenna assembly.

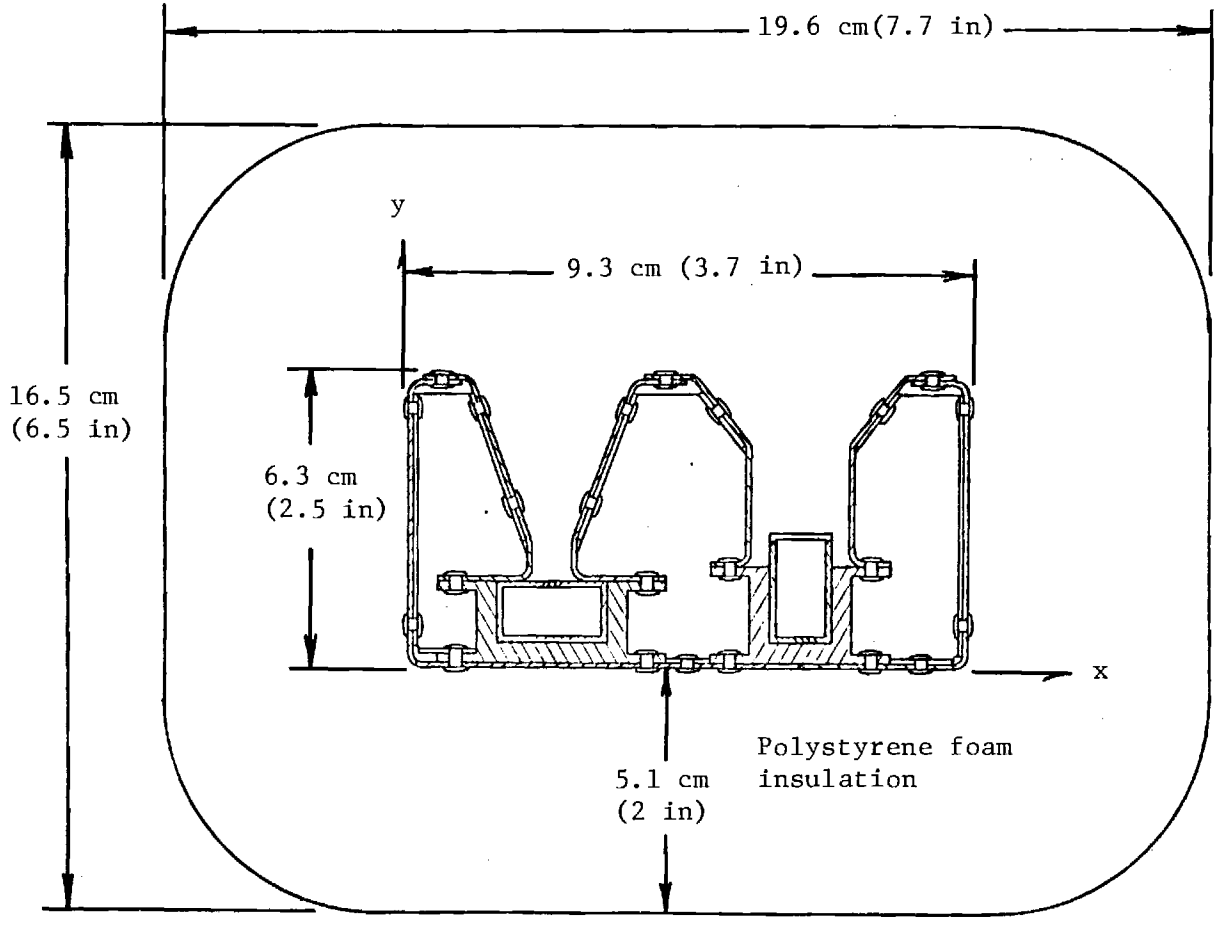

Material: 0.76 millimeter (0.030 inch) aluminum sheet.
Length: 2.54 meters (100 inches)

Figure 8. Insulated Mode II scatterometer assembly cross section.

2. Thermal Analysis

During ascent and after deployment in orbit, the scatterometer antennas will experience adverse thermal environments which will produce temperature gradients within the antennas. The effects of the resulting thermal expansion can cause severe dimensional deformation. In this section, the thermal considerations applicable to the design of the scatterometer antennas are discussed. The analysis necessary for the prediction of the thermal history of the antennas is presented with its resulting effect on the antenna design.

The orbital environment offers the most stringent requirements on the thermal design of the antennas. During ascent, heat produced by aerodynamic heating of the spacecraft is transferred in varying amounts to the payload. This effect is small when compared to the cyclic temperature effects after orbital deployment. The deployed configuration is therefore taken as the limiting design criterion.

a. Orbital Heat Flux

In the vacuum of space the primary heat transfer mechanism is that of radiation, as opposed to conduction or convection. The antennas lose thermal energy by radiation to the infinite heat sink of outer space and receive energy by radiation from the sun and the earth. The total thermal energy incident on the antennas is of three types: (1) direct solar radiation, (2) albedo, and (3) earth thermal radiation. Direct solar irradiance just outside the earth's atmosphere varies from 1350 W/m^2 (428 $Btu/hr\text{-}ft^2$) to 1440 W/m^2 (457 $Btu/hr\text{-}ft^2$) [3]. The total irradiance at the earth's mean distance from the sun is referred to as the solar constant. Part of the solar energy incident on the earth is scattered by the atmosphere and reflected from clouds and terrain; the ratio of this net emergent energy flux to the incident solar energy flux is called albedo. The earth's albedo varies from

0.34 to 0.5 depending on latitude and cloud cover. The long wavelength infrared radiation emitted by the earth due to its temperature varies from 151 W/m^2 (48 $Btu/hr\text{-}ft^2$) to 230 W/m^2 (73 $Btu/hr\text{-}ft^2$) [4] depending on season and latitude. For engineering calculations the following mean values for the three sources of incident radiation are used:

solar constant = 1390 W/m^2 (442 $Btu/hr\text{-}ft^2$)

albedo = 0.39

earth thermal radiation = 211 W/m^2 (67 $Btu/hr\text{-}ft^2$).

Fundamental to the determination of the orbital temperature history of the deployed antennas is the prediction of the heat flux variation due to incident thermal radiation impingent on the antenna surfaces. The determination of the orbital heat flux incident on the surfaces of the antennas is a function of many variables including the satellite orbit altitude, shape, inclination and prescession angle; the earth's orbital position and inclination, the antenna surface orientation and surface properties, and the position of the satellite in its orbit about the earth. The computer program "Computer Program for Determining the Thermal Environment and Temperature History of Earth Orbiting Space Vehicles" [5] and a UNIVAC 1108 computer were utilized to perform the lengthy calculations.

The Mode I antenna is modeled as an eight-sided prism which is oriented in its orbit with its axis 90° from nadir and 45° from the velocity vector; surface number 1 faces the earth throughout the orbit. The Mode II antenna is modeled as a six-sided prism and is also oriented with its axis 90° to nadir, but its axis is parallel to the velocity vector. The orbit for both is circular with an altitude of 800 km (497 mi) and an inclination of 108°.

When specific heats and masses are input to the computer program, it calculates the resulting mass temperatures. The specific heat of polystyrene

TABLE IV

ANTENNA ORBITAL MODEL SURFACE AREA AND MASS ASSIGNMENTS

Surface	Area, m^2 (ft^2)	Mass, kg (lb)
Mode I		
1	0.47 (5.1)	32 (7.0)
2	0.58 (6.2)	1.0 (2.3)
3	0.53 (5.7)	1.7 (3.7)
4	0.66 (7.1)	3.9 (8.7)
5	0.53 (5.7)	1.7 (3.7)
6	0.58 (6.2)	1.0 (2.3)
7	0.12 (1.3)	.05 (0.1)
8	0.12 (1.3)	.05 (0.1)
Mode II		
1	0.49 (5.3)	3.4 (7.4)
2	0.42 (4.5)	2.8 (6.2)
3	0.49 (5.3)	3.4 (7.4)
4	0.42 (4.5)	2.8 (6.2)
5	0.03 (0.3)	0.2 (0.5)
6	0.03 (0.3)	0.2 (0.5)

foam was used, 0.32 cal/gC° (0.32 Btu/lb-F°) and the mass of the antenna is distributed among the surfaces by an area weighted average. The surfaces and the assigned masses are listed in Table IV.

Two orbital situations are investigated. Orientation I is a hot case; the earth is at the summer solstice with the orbit plane perpendicular to the sun line (see Figure 9) and the northern end of the axis of the earth is tilted 23.5° toward the sun. The antenna remains in the sun during the entire orbit. Orientation II is a cold case; the earth is at the winter solstice with the orbit plane parallel to the sun line and the northern end of the axis of the earth is tilted 23.5° away from the sun. The antenna is in the shadow of the earth for 33.5% of the orbit.

Eight cases of varying infrared emittance, ε, and solar absorbtivity, α_s, were investigated for the two orientations described above. Table V lists the values of α_s and ε considered:

TABLE V

SURFACE COATING CASES CONSIDERED

Case	α_s	ε	α_s/ε	Surface Type
1	0.04	0.85	0.05	Solar Reflector
2	0.27	0.86	0.31	Solar Reflector
3	0.06	0.085	0.74	Flat Reflector
4	0.74	0.86	0.86	Flat Absorber
5	0.25	0.25	1.00	Flat Reflector
6	0.89	0.77	1.15	Flat Absorber
7	0.42	0.21	2.00	Solar Absorber
8	0.27	0.03	9.00	Solar Absorber

The effect of varying the surface coating properties on the integrated average temperature of the Mode I antenna model for Orientations I and II appears in Figure 10; in Figure 11 similar results are given for the Mode II antenna. Figure 12 shows the variation of the average temperature of the

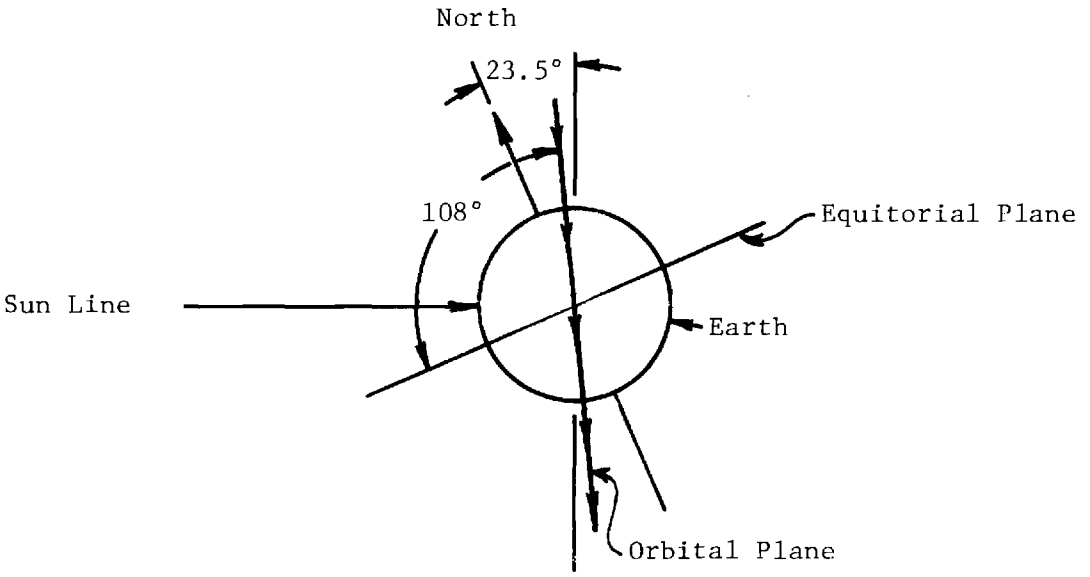

Orbit Orientation I, Summer Solstice

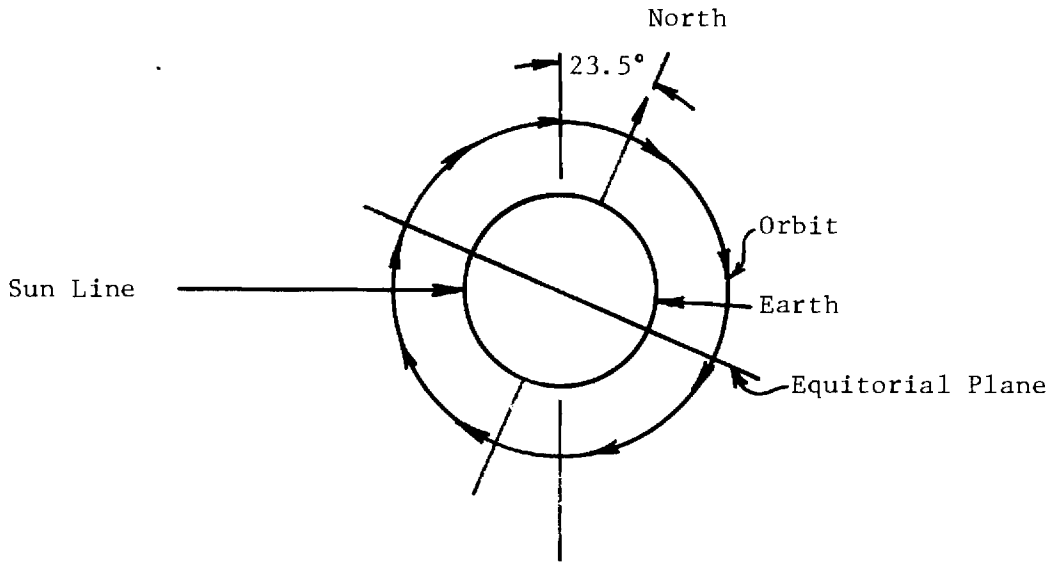

Orbit Orientation II, Winter Solstice

Figure 9. Solar heat flux orbital orientations.

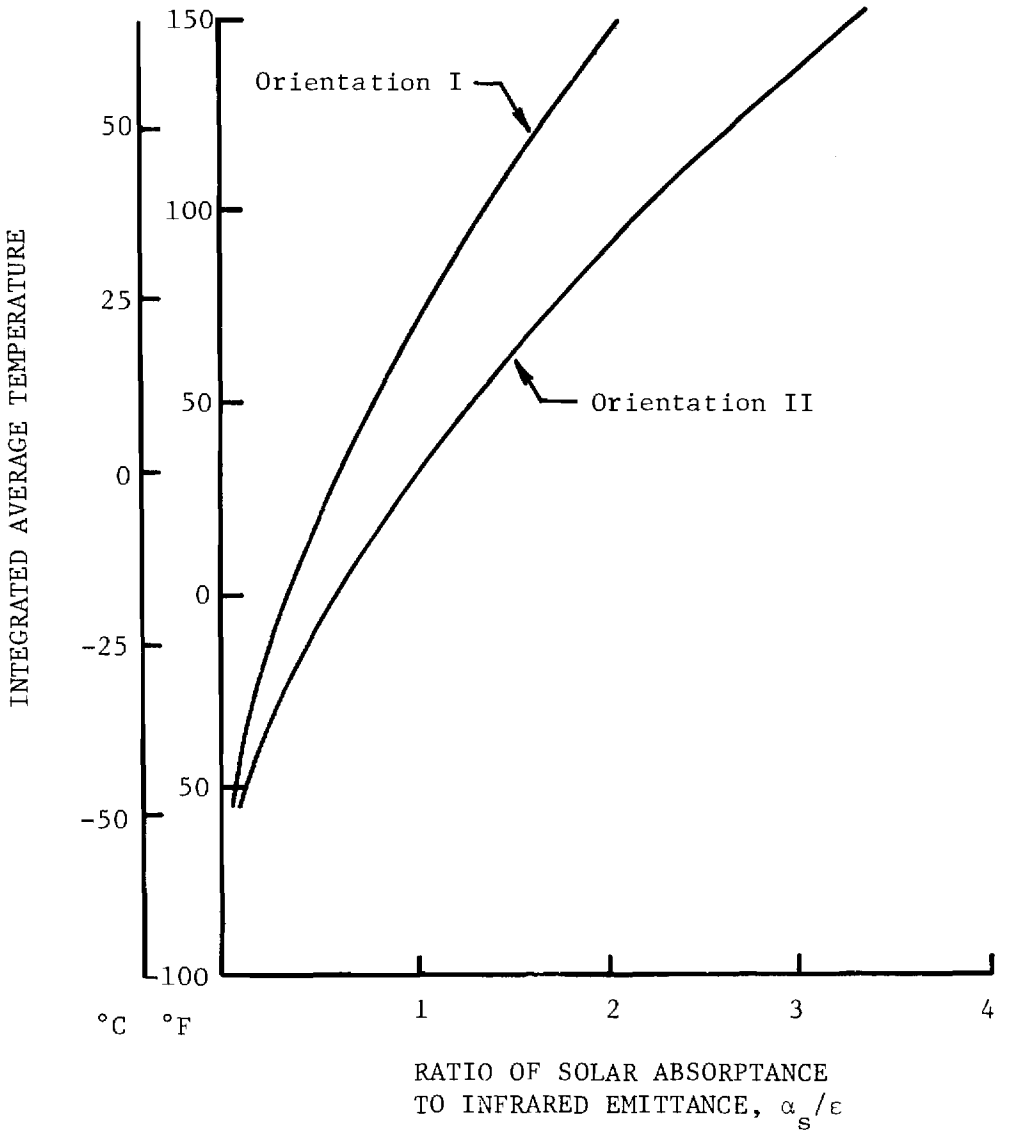

Figure 10. Effect of α_s/ε ratio on average Mode I antenna temperature.

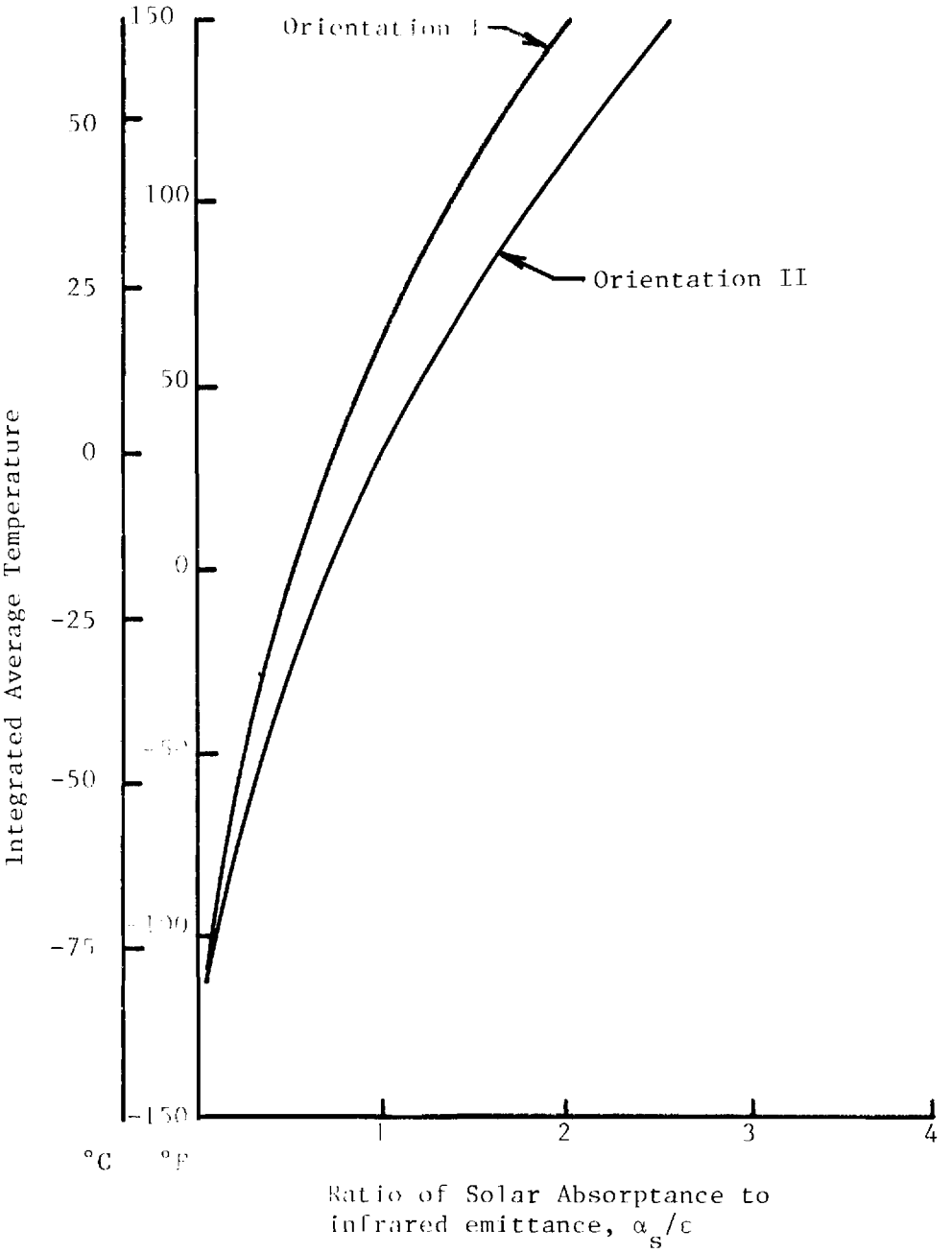

Figure 11. Effect of α_s/ε ratio on average Mode II antenna temperature.

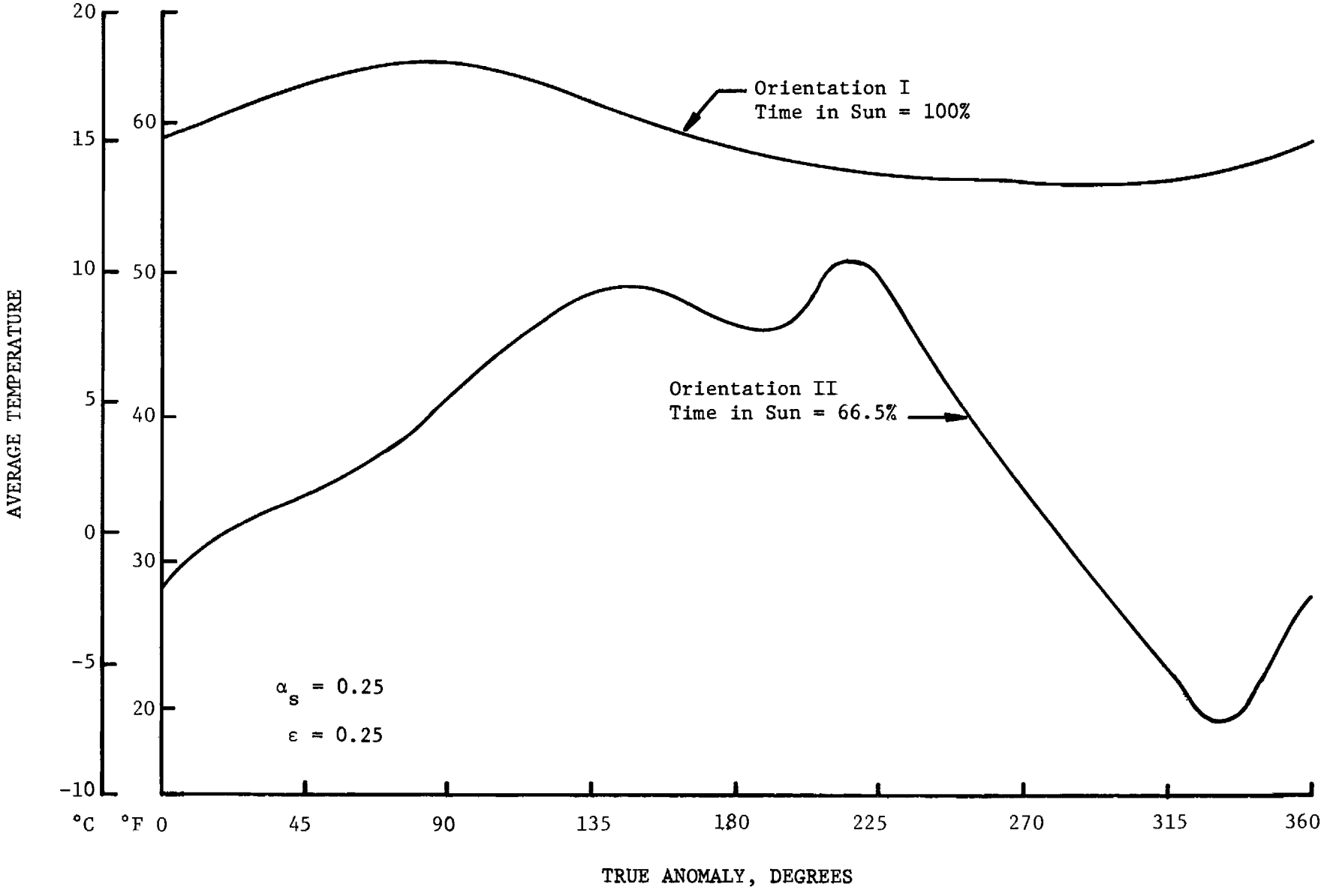

Figure 12. Orbital temperature variation of the Mode I scatterometer antenna

Mode I antenna model during an orbit for $\alpha_s/\varepsilon = 1.00$ (See Table V, case 5); Figure 13 presents this temperature variation for the Mode II antenna. The temperatures are based on area, mass, specific heat, emittance, and absorptance of an isolated antenna. Conduction of heat within the antenna and thermal exchange with the sensor module are not included. The primary purpose of this analysis is the generation of orbital heat flux variations for use as input to the heat conduction antenna model described in Section II-C-2-b.

b. Thermal Gradients

To investigate the heat transfer within the scatterometer antennas, each antenna was modeled by an electrical analog and programmed for computer solution using the "Systems Improved Numerical Differencing Analyzer" (SINDA) [6] computer program. SINDA utilizes the lumped-parameter method of thermal system solution. To apply the method to a heat-conduction problem the system is divided into a number of small but finite subvolumes; a reference number is assigned to each. Each subvolume is assumed to be at the temperature corresponding to its center and the physical system is replaced by a network of fictitious heat-conducting rods between the centers, or nodal points, of the subvolumes. The thermal conductance corresponding to the conductance of the material between nodal points is assigned to each rod so that the network approximates the heat flow in the continuous system.

An 85 node three-dimensional model was prepared for the Mode I antenna. The antenna was divided along its length into 51 cm (20 inch) long sections. These are referred to as "stations" in Figure 14. Each station was further subdivided in a plane transverse to the long dimension of the antenna to model internal heat flow as indicated in Figure 15. The nodes were numbered to reflect their location within the model. The first digit of the three digit nodal number indicates the station (see Figure 14); the remaining two digits reflect the cross-sectional location (see Figure 15). A total of 266 thermal

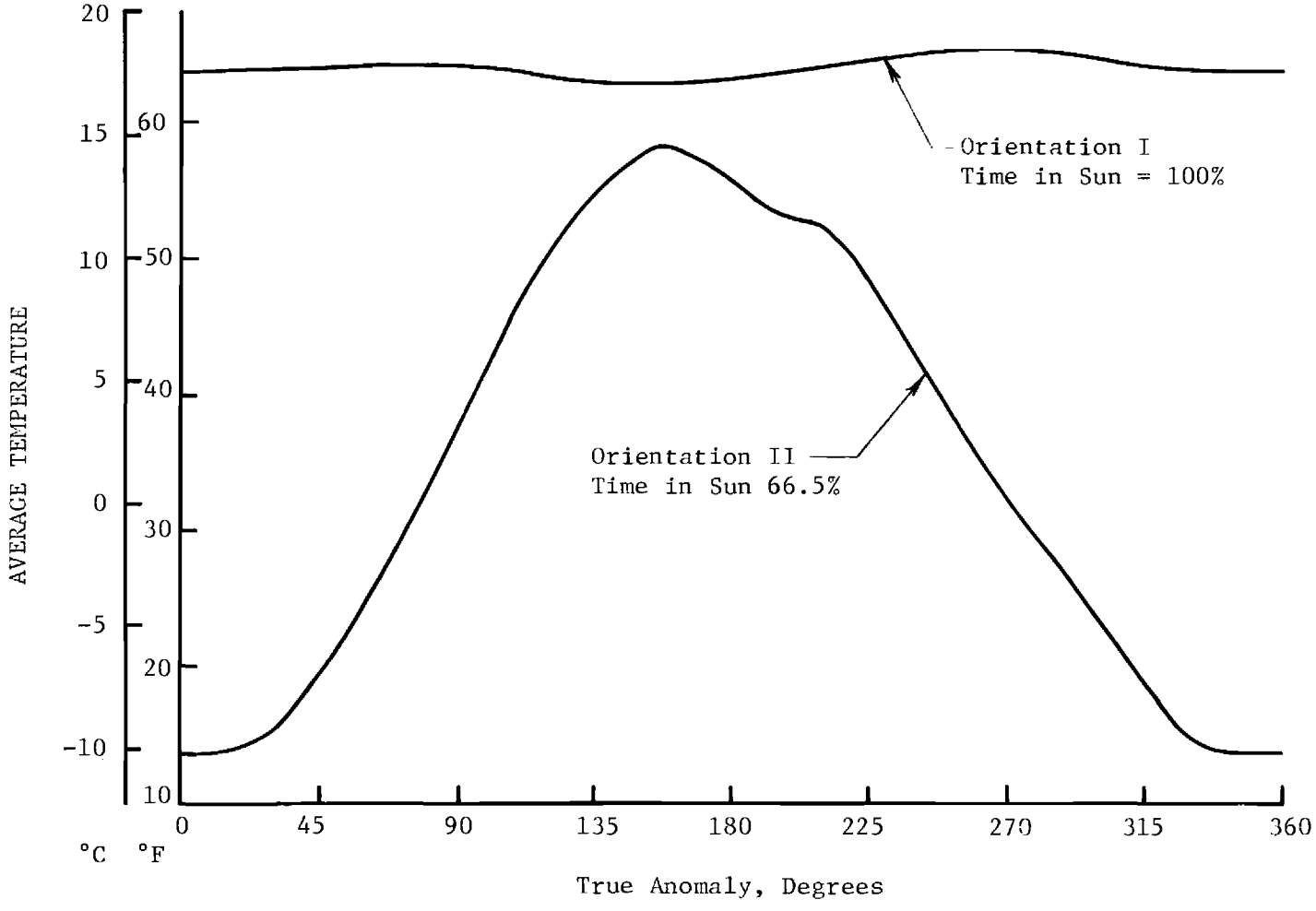

Figure 13. Orbital temperature variation of the Mode II scatterometer antenna.

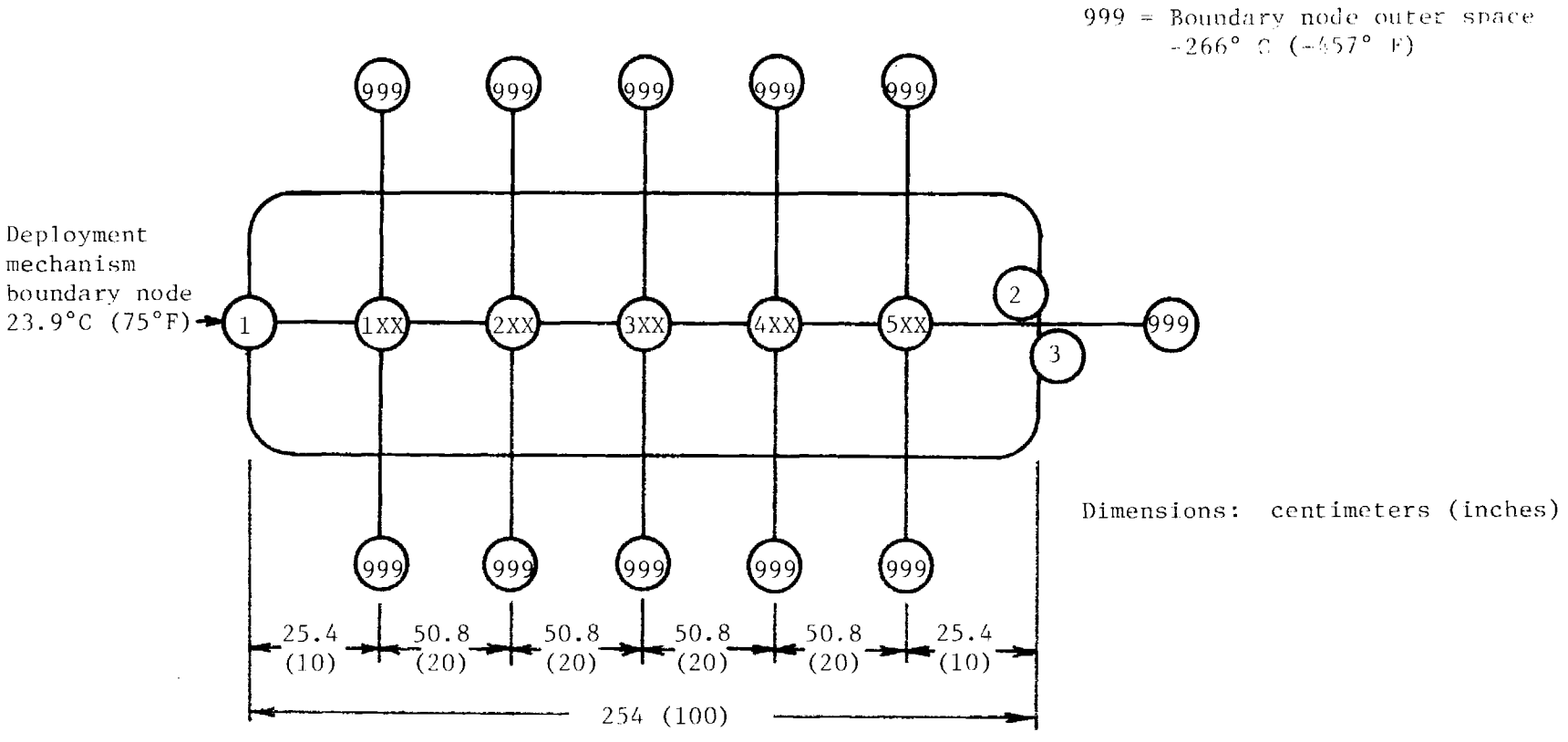

Thermal model station locations
(see Figure 15 for station cross section)

Figure 14. Thermal model nodal assignments for the Mode I antenna.

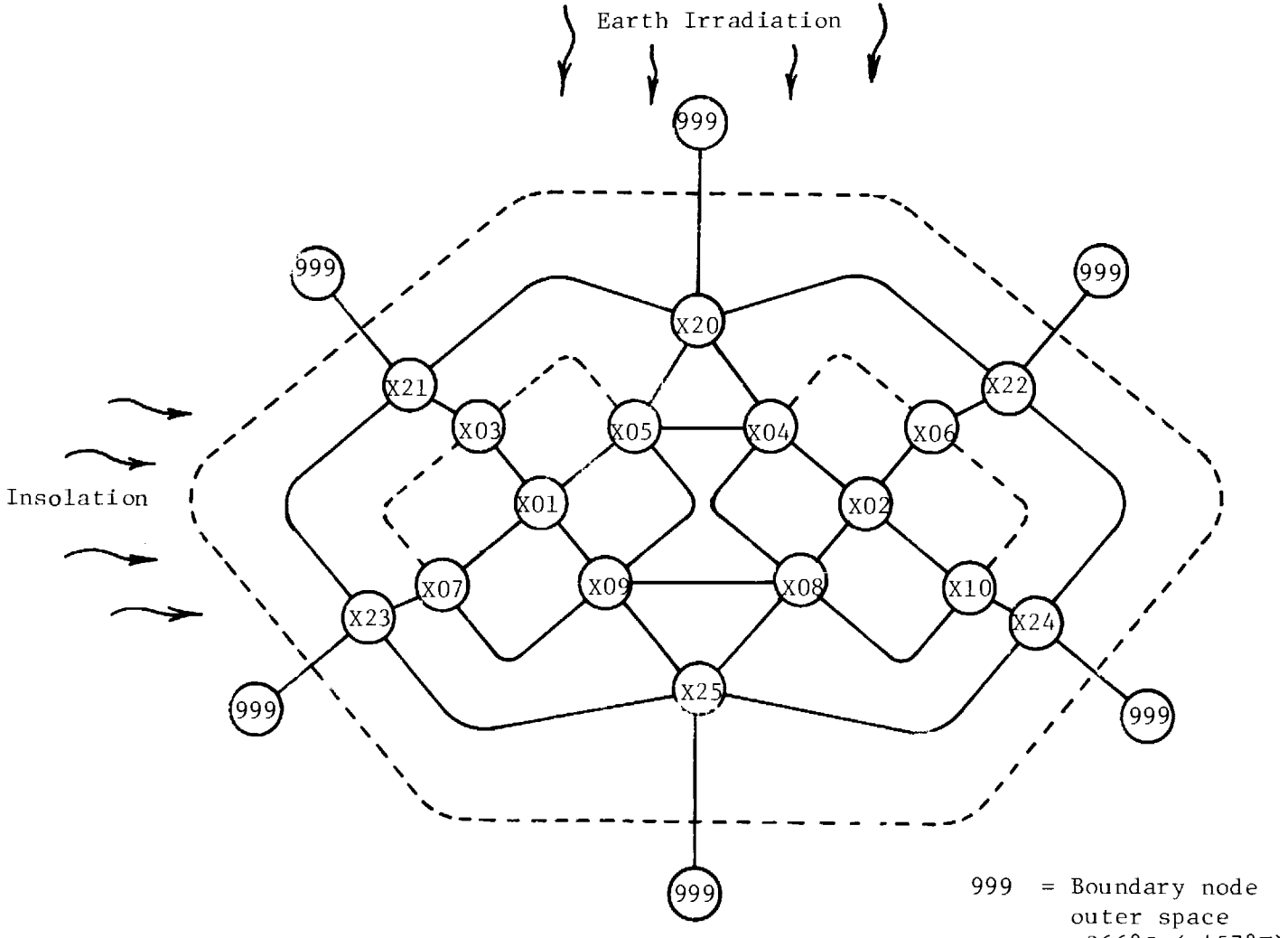

Figure 15. Thermal model nodal assignments for the Mode I scatterometer antenna.

conductors were required to model the thermal paths connecting the 85 nodes. The radiation input to the antenna from the earth and sun took the values stated in Section II-C-2-a and the directions indicated in Figure 15. A value of 0.86 for the infrared emittance and a value of 0.2 for the solar absorptance of the exterior surfaces were used. The thermal conductance of aluminum was taken as 7.3 cal/min-cm-C° (8 Btu/hr in F°) and that for styrofoam, 1.6×10^{-3} cal/min-cm-C° (1.7×10^{-3} Btu/hr in F°).

The temperature distribution resulting from this analysis appears in Figures 16 through 18. The legend in Figure 16 indicates the method used in these figures for displaying the temperatures. Each box represents a node, and the number in the upper left corner is the node number. The number 324, for example, refers to station 3 (Figure 14) and cross section location 24 (Figure 15). The remaining numbers in the boxes are nodal temperatures in degrees Celcius and, in parentheses, degrees Fahrenheit. The external surface temperature of the antenna appears in Figure 16 (cross sectional nodes 20 through 25) for the 5 nodal stations. Figure 17 shows the temperature distribution at the aluminum skin of the antenna (cross sectional nodes 03 through 10), and Figure 18 gives the temperature at the central nodal points (nodes X01 and X02). The deployment mechanism was modeled as a constant temperature boundary node at an arbitrarily chosen temperature of 23.9° C (75° F). Notice that the internal temperature of the antennas varies little from the temperature of the deployment mechanism (Figure 18). Outer space is represented by node number 999 at a constant temperature of -266° C (-457° F).

3. Mechanical Analysis

This section presents predictions for the natural frequency, moment of inertia, and section modulus for the Mode I and Mode II antennas. The manufacturing tolerances are discussed and the tolerance budget is presented.

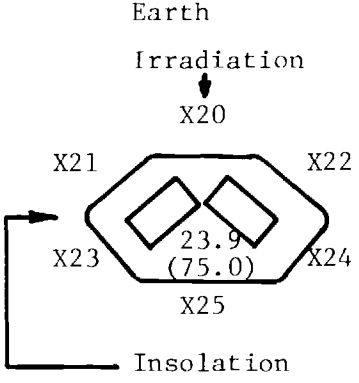

121 6.0 (42.8)	221 5.7 (42.2)	321 5.7 (42.2)	421 5.7 (42.2)	521 5.9 (42.7)
120 -28.1 (-18.6)	220 -29.8 (-21.7)	320 -29.9 (21.8)	420 -29.8 (21.7)	520 -28.2 (-18.8)
122 -43.8 (-46.8)	222 -45.6 (-50.1)	322 -45.6 (-50.1)	422 -45.6 (-50.1)	522 -43.8 (-46.9)
124 -91.3 (-132.3)	224 -95.9 (-140.6)	324 -95.9 (-140.7)	424 -95.9 (-140.6)	524 -91.4 (-132.5)
125 -90.2 (-130.4)	225 -97.6 (-143.7)	325 -97.7 (-143.8)	425 -97.6 (-143.7)	525 -90.4 (-130.7)
123 -22.4 (-8.3)	223 -23.4 (-10.2)	323 -23.4 (-10.2)	423 -23.4 (-10.2)	523 -22.4 (-8.4)

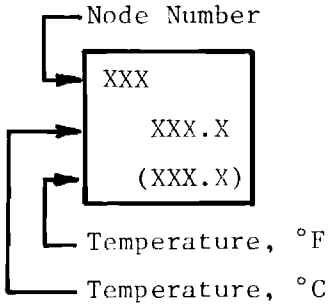

LEGEND

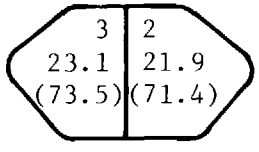

$\alpha_s = 0.2$

$\varepsilon = 0.2$

Figure 16. Mode I scatterometer antenna exterior surface temperature distribution.

103 23.5 (74.3)	203 23.4 (74.2)	303 23.4 (74.2)	403 23.4 (74.2)	503 23.2 (73.8)
105 23.1 (73.5)	205 22.9 (73.2)	305 22.9 (73.2)	405 22.8 (73.1)	505 22.6 (72.6)
104 23.1 (73.6)	204 22.9 (73.3)	304 22.9 (73.3)	404 22.9 (73.3)	504 23.0 (73.4)
106 16.9 (62.4)	206 15.7 (60.2)	306 15.7 (60.2)	406 15.7 (60.2)	506 16.7 (62.1)
110 23.3 (74.0)	210 23.2 (73.8)	310 23.2 (73.8)	410 23.2 (73.8)	510 23.3 (73.9)
108 22.3 (72.2)	208 22.0 (71.6)	308 22.0 (71.6)	408 22.0 (71.6)	508 22.2 (72.0)
109 23.6 (74.5)	209 23.6 (74.4)	309 23.6 (74.4)	409 23.6 (74.4)	509 23.3 (74.0)
107 22.6 (72.6)	207 22.2 (72.0)	307 22.2 (72.0)	407 22.3 (72.1)	507 22.0 (71.6)

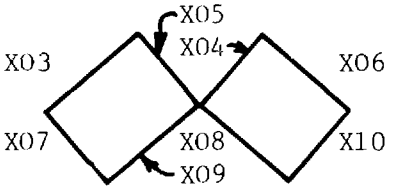

Figure 17. Mode I scatterometer antenna surface temperature distribution.

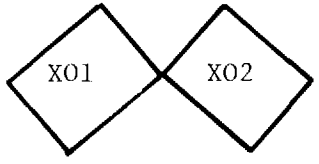

101 23.6 (74.5)	201 23.6 (74.5)	301 23.6 (74.4)	401 23.6 (74.5)	501 23.3 (74.0)
102 23.3 (74.0)	202 23.2 (73.8)	302 23.2 (73.8)	402 23.2 (73.8)	502 23.3 (73.9)

Figure 18. Mode I scatterometer antenna interior temperature distribution.

a. Stowed and Deployed Design Criteria

The scatterometer antennas in the stowed (launch) configuration will appear as indicated in Figure 1. The antennas are analyzed for a three point tie-down arrangement in Section II-C-3-c. The three point analysis considers anchor placement at the deployment mechanism, and the sensor module/bus interface, and at the "free" end of the antennas. The thermal analysis takes the deployed configuration to be the limiting environmental criterion for the thermal design of the antennas.

b. Antenna Mass and Sectional Properties

The sectional properties of the Mode I and Mode II scatterometer antennas appear in Table VI. The coordinates are as shown in Figure 6 and 8. The centroidal parameters c_x and c_y represent the distance from the centroid to the outer surfaces of the aluminum antennas; these values do not include the styrofoam insulation. Likewise, the moment of inertia, I, and the section modulus, Z, are calculated for the basic aluminum antennas.

TABLE VI

MASS AND SECTION PROPERTIES OF THE SCATTEROMETER ANTENNA

	Mode I	Mode II
C_x	5.85 cm (2.31 in)	4.65 cm (1.83 in)
I_x	134.4 cm^4 (3.23 in^4)	57.4 cm^4 (1.38 in^4)
Z_x	22.9 cm^3(1.40 in^3)	12.3 cm^3 (0.75 in^3)
C_y	3.0 cm (1.18 in)	1.4 cm (0.55 in)
I_y	65.8 cm^4 (1.58 in^4)	18.3 cm^4 (0.44 in^4)
Z_y	22.0 cm^3 (1.34 in^3)	13.1 cm^3 (0.80 in^3)

The estimated mass breakdown of the scatterometer antennas is listed in Table VII. This estimate does not include the deployment mechanism. The styrofoam mass is calculated assuming the maximum 7.4 cm (2.9 in) insulation

TABLE VII

ESTIMATED MASS OF THE MODE I AND MODE II SCATTEROMETER ANTENNAS

Component	Mass, kg (lbs)	
	Mode I	Mode II
Edgeslot horn plate	1.0 (2.1)	0.4 (0.9)
Broadwall horn plate	1.1 (2.4)	0.5 (1.2)
Skin	1.7 (3.8)	1.2 (2.6)
Edgeslot extrusion	1.1 (2.5)	1.1 (2.5)
Broadwall extrusion	1.3 (2.8)	1.3 (2.8)
Ribs (21)	0.5 (1.1)	0.3 (0.6)
Rivets	0.2 (0.4)	0.1 (0.3)
Hinge, anchors, end plates	0.1 (0.3)	0.1 (0.2)
Waveguide (2)	0.7 (1.6)	0.7 (1.6)
	0.1 (0.1)	0.1 (0.1)
Total (ea structure)	7.7 (17.0)	5.7 (12.7)
Total structure per unit	15.4 (34.0)	5.7 (12.7)
Insulation	7.7 (17.0)	6.9 (15.3)
Paint, adhesive	0.1 (0.1)	0.1 (0.1)
Total per unit	23.2 (51.1)	12.7 (28.1)
Total for system	59.1 (130.3)	

thickness for the Mode I antennas; a 5.1 cm (2 in) thickness is assumed for the Mode II mass estimate.

c. Natural Frequency

For deflection and natural frequency calculations the antenna is modeled as a redundantly supported beam. Simple supports are taken at each end (x=0 and x=254 cm), with a third support at x = 80 cm (31.5 in). The load, W, is assumed evenly distributed along the length of the beam. Figure 19 indicates the generalized deflection, $\delta I/W$ along the antenna. The maximum deflection, δ_{max}, is given by

$$\delta_{max} = 1.33 \times 10^{-4} \frac{W}{I} .$$

The natural frequency of the antennas is found by utilizing the Rayleigh energy method. The deflection curve of Figure 19 is approximated by using four sine wave segments, and equations are written for the deflection in terms of a summation of the four segments. The kinetic energy, KE, is calculated using the relation

$$KE = \frac{1}{2} \rho\omega^2 \int A^2 Y^2 dx ,$$

and the potential energy, PE, by

$$PE = \frac{1}{2} EI \int \left(\frac{d^2Y}{dx^2} \right)^2 dx ,$$

where

ρ = density

ω = natural frequency

A = cross sectional area

Y = Y(x) = deflection curve

x = axial dimension

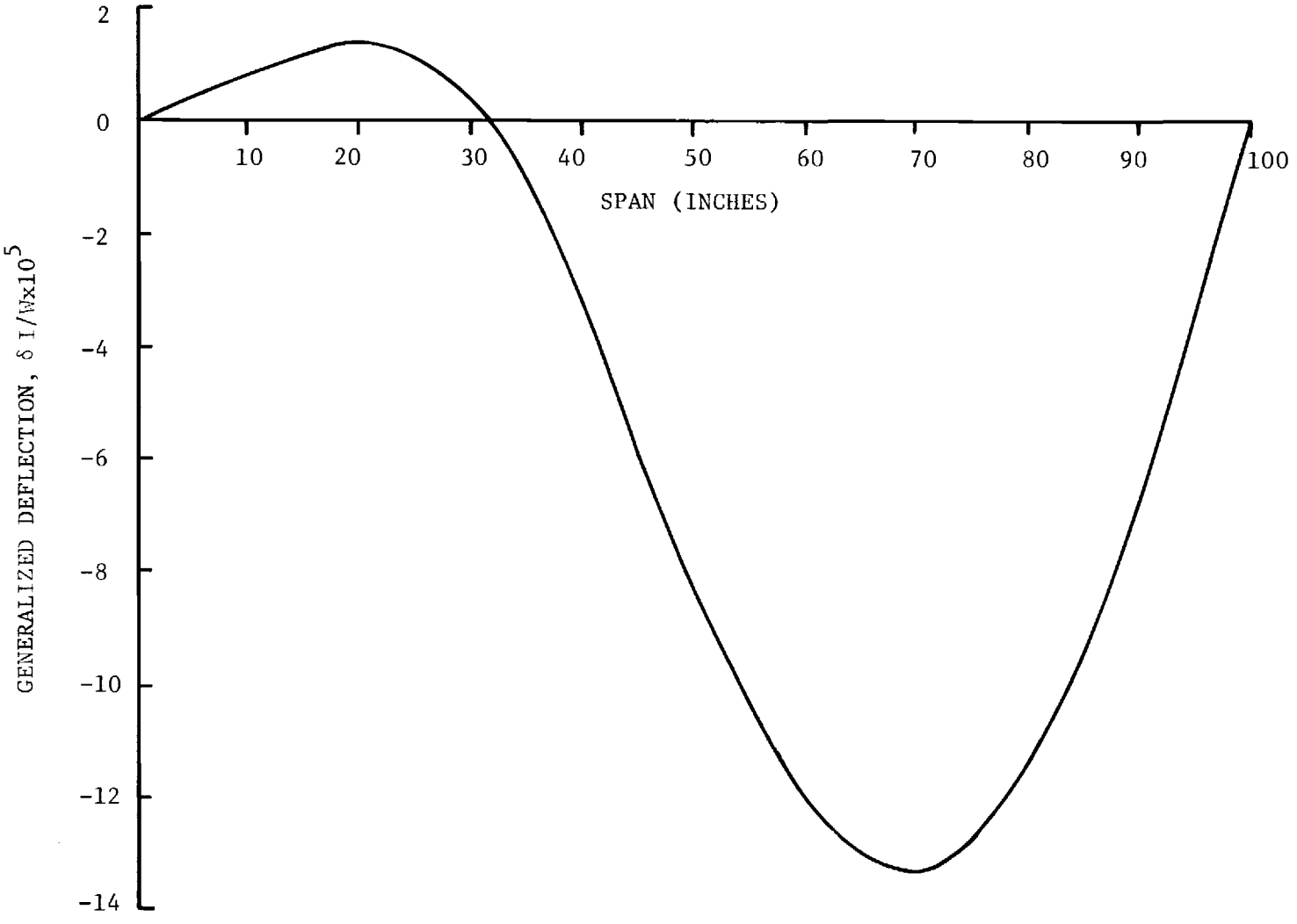

Figure 19. Generalized deflection curve for the Mode 1 scatterometer antenna.

E = Young's modulus

I = moment of inertia.

Equating the kinetic and potential energies and solving for ω yields a natural frequency of 85.6 Hz for the insulated Mode I dual-antenna assembly.

d. Tolerance Budget Evaluation

In this section are presented the mechanical tolerances which must be maintained in order to insure proper electrical performance of the scatterometer antennas. Included is a discussion of the tolerances which will be used in the manufacture of the component parts of the antennas and the methods which will be employed to insure that these tolerances are achieved. The distortion to be expected from thermal effects is analyzed and the deformation resulting from launch induced internal stress is also investigated.

The waveguide slots are to be machined using a 2-axis numerically controlled milling machine thereby maintaining linear dimensional accuracy to within $\pm$0.0013 cm ($\pm$0.005 in). The straightness of the waveguides is insured by the extrusion mounting arrangement (see Section II-C-1).

The aluminum sheeting is to be 2024 aluminum, which has essentially a zero minimum bending radius. Suitable fixtures are to be fabricated for the bending and assembly operations. Rivet placement will insure dimensional accuracy, and Coulomb friction inherent in riveted structures will aid in lowering the vibrational transmissibility of the antennas.

The antennas are to be isolated thermally from the solar and terrestrial heat inputs by a thermal control surface coating and styrofoam insulation. The tolerance to be held over the length of the antennas is 0.1 cm (0.04 in). The expansion, δ, of a material due to a temperature change, ΔT, is given by

$$\delta = L\alpha\Delta T$$

where α = coefficient of thermal expansion and L = original length. The

coefficient of thermal expansion for aluminum is 12.8×10^{-6} 1/F°. Assuming a maximum thermal expansion, δ, of 0.1 cm (0.04 in) over the length of the antenna, L = 254 cm (100 in), the above equation yields a maximum ΔT of 31.3° F (17.4° C). The temperature change across the antenna, therefore, must be kept below about 17° C to maintain a maximum difference of 0.1 cm in the length of the sides of the antenna. The analysis presented in Section II-C-2-b for a 23.9° C (75° F) deployment mechanism interface temperature indicates that 17° C (31° F) can be maintained.

The stress, σ, experienced by an axially loaded member with cross sectional area, A, under a load, P, is given by $\sigma = P/A$. If one is confined to body forces (acceleration forces) only, then P = ma, where m is the mass of the member and a is the axial acceleration. The mass is given by the product of the density, ρ, the cross sectional area, A, and the member length, L. The load is then given by $P = \rho ALa$ and the stress by $\sigma = \rho La$. Applying the above equation to a scatterometer antenna in the launch configuration and assuming a 100 g acceleration gives

ρ = 2.8 g/cc (0.1 lb/in^3),

L = 254 cm (100 in), and

a = 980 m/sec^2 (3220 ft/sec^2).

Substituting the above values into the stress equation yields a stress of 689 N/cm^2 (1×10^3 psi). The antenna will not deform permanently until it is stressed beyond its tensile yield strength, which for aluminum is approximately 34×10^3 N/cm^2 (50×10^3 psi). The antennas can, therefore, withstand axial acceleration loading without becoming permanently deformed.

The relation between stress, σ, and strain, ε, is given by $E = \frac{\sigma}{\varepsilon}$ where E is Young's modulus. Young's modulus for aluminum is about 6.9×10^6 N/cm^2 (10×10^6 psi). Using the above stress of 689 N/cm^2 (1×10^3 psi), associated with a 100 g acceleration, the strain, ε, by the above equation is 1×10^{-4}

cm/cm (in/in). Deflection, δ, is given by $\delta = \varepsilon L$. For the 254 cm (100 in) scatterometer antenna the deflection is 0.03 cm (0.01 in).

4. Comparison of Predicted and Required Performance

a. Envelope

The proposed Mode I and Mode II scatterometer antenna physical dimensions are displayed in Figures 7 and 8, respectively. The available space accommodations are also detailed in these drawings and the overall clearance envelope for the antenna system in the launch configuration appears in Figure 16.

The maximum allowed styrofoam insulation thickness is 7.4 cm (2.9 in). Use of this insulator creates essentially isothermal conditions within the aluminum antennas (see Figure 15). Optimization of the insulation may result in a reduction in the required thickness.

b. Mass

The design goal for the individual scatterometer antennas is 13.6 kilograms (30 lbs); the estimated mass breakdown appears in Table VII. The Mode I dual-antenna (4 horns) insulated units may have a maximum mass of 27.2 (60 lbs) each. There are to be four Mode I antennas (two dual-antenna units) and a single Mode II antenna, for a total design goal of 68.0 kilograms (150 lbs) for the scatterometer system. The estimated mass for the present design is 59.1 kilograms (130.3 lbs).

c. Environmental

The environmental performance requirements are presented in Table II. The investigation of the antenna response to the thermal environment is detailed in Section II-C-2-b. Mechanical characteristics are presented in Section II-C-3.

III. ANTENNA TESTS

Antenna pattern tests and VSWR and isolation tests were performed on full frequency, quarter-length brassboard models to determine the quality of the final array design and verify the feasibility of producing full-length brassboard antennas which would satisfy the desired performance criteria. Quarter-length models were used in order to reduce the number of waveguide slots that had to be cut in each array and to produce a smaller antenna to simplify testing. The net result is that the narrow beamwidth (azimuth) is four times as large as that of the full-size array (2.0° vs. 0.5°).

In the case of the full-length arrays, the individual slots near the center of the array will have quite small displacements (broadwall array) or tilt angles (edge slot array); however, in the case of the quarter-length models which are designed for the same efficiency and aperture taper, the center slots will be highly displaced or tilted. Therefore, for proper testing it was deemed necessary to fabricate two versions of each array. Two arrays of each type (broadwall slots and edge slots) were fabricated; one array was an "efficient" design which was designed to dissipate about 10% of the incident power in the load while the other was an "inefficient" design which dissipates over 50% of the incident power in the load.

The inefficient edge slot array design produces cross-polarization levels (because of the smaller slot angles) which are more representative of those to be obtained in the full-length arrays, while the efficient design of both antennas will provide a good measure of the gain which will be obtained in the full length antenna. The gain of the final full-length array will be 6 dB higher due to the 4:1 beamwidth ratio in the azimuth plane. The smaller slot displacements of the inefficient broadwall slot array enable manufacturing techniques and tolerances to be realistically evaluated. Both the efficient

and inefficient arrays of each type should have the same beamwidth and sidelobe levels, since the aperture distribution is theoretically the same in both cases.

The performance requirements specified for the Mode I antennas are listed in Table VIII. The azimuth beamwidth for the quarter-length arrays tested will, of course, be four times as large as that specified for the full-length arrays, i.e., 2.0°.

Tables IX and X present a tabulation of the results of the antenna pattern tests for the inefficient and efficient designs, respectively. The position of the peak of the beam was determined by selecting a reference level on expanded angle plots (-10 dB, in fact) and calling the beam peak the location half-way between the -10 dB crossings. The elevation pattern slope was calculated by approximating the tangent to the pattern as a straight line over a small angular increment about the measurement point ($\pm$19.5°).

Azimuth and elevation antenna patterns are shown in Figures 20 through 43, while typical VSWR data are shown in Figures 44, 45, and 46. In all cases the upper trace is the parallel polarized pattern and the lower one is the cross polarized pattern. The isolation between the two input channels (vertical and horizontal polarizations) was measured and found to be in excess of 40 dB.

It is apparent from the antenna pattern data that there are three areas in which the quarter-length brassboards do not meet the antenna specifications of Table I. These three areas are discussed below and actions which could be undertaken to solve these problems are presented.

1. Broadwall Slot Array Elevation Sidelobes - Since the aperture illumination in this plane of the broadwall slot array is essentially uniform (indicating -13.2 dB sidelobes), the problem apparently lies in excessive phase error across the aperture

TABLE VIII

SEASAT-A MODE I SCATTEROMETER ANTENNA REQUIREMENTS

Parameter	Mode I Antenna
Frequency	14.595 GHz
Bandwidth	$\pm$1 MHz
3-dB Beamwidth	0.5° (2.0°) Az by 25° El*
Power Gain	32.5 dBi peak 25 dBi @ $\pm$19.5° El
Elevation Pattern Slope	$\leq$1.0 dB/° over $\pm$19.5° El
Polarization	Vertical and Horizontal Cross Pol $\leq$ -20 dB
Sidelobe Levels	-20 dB Az -12 dB El
Isolation Between Vertical/Horizontal Antennas	>20 dB
VSWR	$\leq$1.3:1

*Nominal beamwidths. The narrow beamwidth is 2.0° for the quarter-length models and 0.5° for the full-length models.

TABLE IX

SLOT ARRAY DATA
(INEFFICIENT DESIGN)

Edge Slot Array

	Azimuth Cut				Elevation Cut				Gain (Add 6 dB)	
Frequency	BW	SLL	X Pol.	Beam Pos.	BW	SLL	X Pol.	Pat. Slope	Beam Peak	$\pm$19.5°
14.55 GHz	2.05	-18.6	-23.3	4.6	28.0	-40	-20.1	0.68	NA	NA
14.60	2.05	-19.0	-21.7	4.8	27.5	-40	-20.3	0.71	NA	NA
14.65	2.05	-19.2	-24.0	5.0	27.5	-40	-22.8	0.67	NA	NA

Broadwall Slot Array

	Azimuth Cut				Elevation Cut				Gain (Add 6 dB)	
Frequency	BW	SLL	X Pol.	Beam Pos.	BW	SLL	X Pol.	Pat. Slope	Beam Peak	$\pm$19.5°
14.55 GHz	2.05	-21.8	-18.7	4.7	27.0	-11.9	-18.8	0.69	NA	NA
14.60	2.05	-21.6	-19.7	4.9	27.0	-11.8	-17.8	0.70	NA	NA
14.65	2.05	-21.1	-20.3	5.2	27.0	-11.9	-19.3	0.70	NA	NA
Spec.	2.0	-20	-20	<8	25.0	-12	-20	<1.0	32.5	25.0

Note: BW and Beam Pos. in degrees; SLL, X Pol., and Gain in dB; Pat. Slope in dB/degree.

TABLE X

SLOT ARRAY DATA
(EFFICIENT DESIGN)

Edge Slot Array

	Azimuth Cut				Elevation Cut				Gain (Add 6 dB)	
Frequency	BW	SLL	X Pol.	Beam Pos.	BW	SLL	X Pol.	Pat. Slope	Beam Peak	±19.5°
14.55 GHz	2.10	-19.4	NA	4.4	27.0	-40	NA	0.66	27.9	21.5
14.60	2.10	-19.3	NA	4.7	27.0	-40	NA	0.67	27.9	21.5
14.65	2.10	-19.2	NA	5.0	27.5	-40	NA	0.68	27.9	21.5

Broadwall Slot Array

	Azimuth Cut				Elevation Cut				Gain (Add 6 dB)	
Frequency	BW	SLL	X Pol.	Beam Pos.	BW	SLL	X Pol.	Pat. Slope	Beam Peak	±19.5°
14.55 GHz	2.05	-21.7	NA	4.7	28.2	-11.8	NA	0.67	27.3	21.0
14.60	2.10	-22.8	NA	4.9	28.0	-11.9	NA	0.67	27.3	20.7
14.65	2.05	-23.0	NA	5.1	27.0	-11.9	NA	0.73	27.7	21.0
Spec.	2.0	-20	-20	<8	25.0	-12	-20	<1.0	32.5	25.0

Note: BW and Beam Pos. in degrees; SLL, X Pol., and Gain in dB; Pat. Slope in dB/degree.

due to the horn flare. The solution is simply to make the horn flare length longer, thereby reducing the aperture phase error. The impact of such a change on the mechanical design would have to be given careful attention.

2. Cross-Polarization - Although the measured data do not meet the -20 dB specifications in all cases (consider only the inefficient design), there appears to be an inconsistency in these data. It is believed that the test range set-up is at fault here and that the worst case cross-polarized lobes (about -18 dB) are likely caused by ground reflections on the antenna test range. Additional work should be performed on establishing a more accurate cross-polarization measurement technique.

3. Edge Slot Array Azimuth Sidelobes - It is believed that the high level of these sidelobes is a result of inaccurate measurement of slot conductance and the corresponding error in the resulting aperture distribution, since the array design procedure is otherwise the same for both the edge slot and broadwall slot arrays. Further measurements should be performed and the edge slot conductance model refined in order to implement an array design which will produce acceptable sidelobes.

None of the problem items listed above are a result of basic limitations in the capabilities of the chosen antenna design, and EES feels that the antenna performance can be brought into concordance with specifications with only a minimum level of effort.

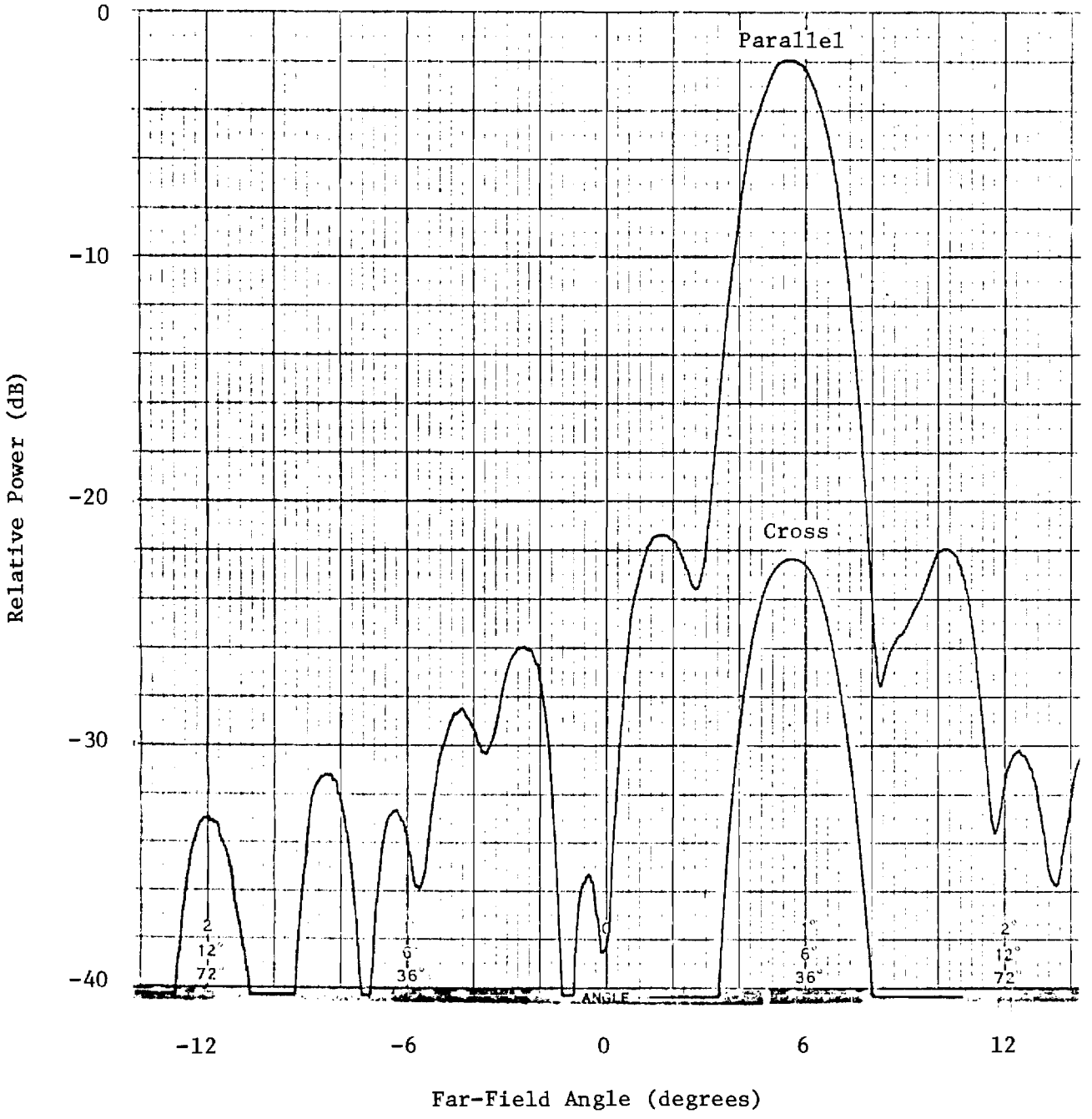

Figure 20. Far-field azimuth pattern for the edge-slot array antenna at 14.55 GHz; efficient design.

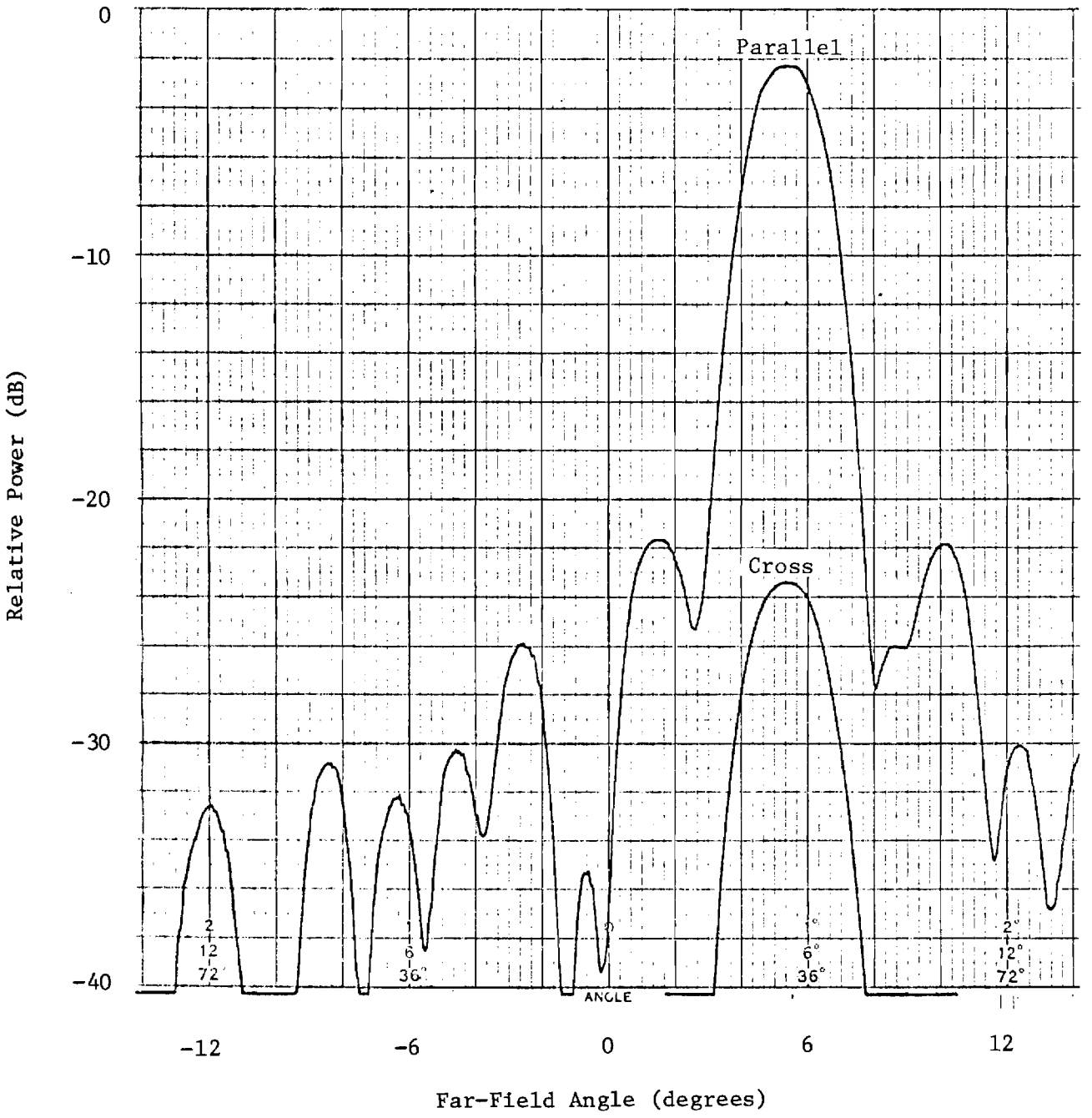

Figure 21. Far-field azimuth pattern for the edge-slot array antenna at 14.60 GHz; efficient design.

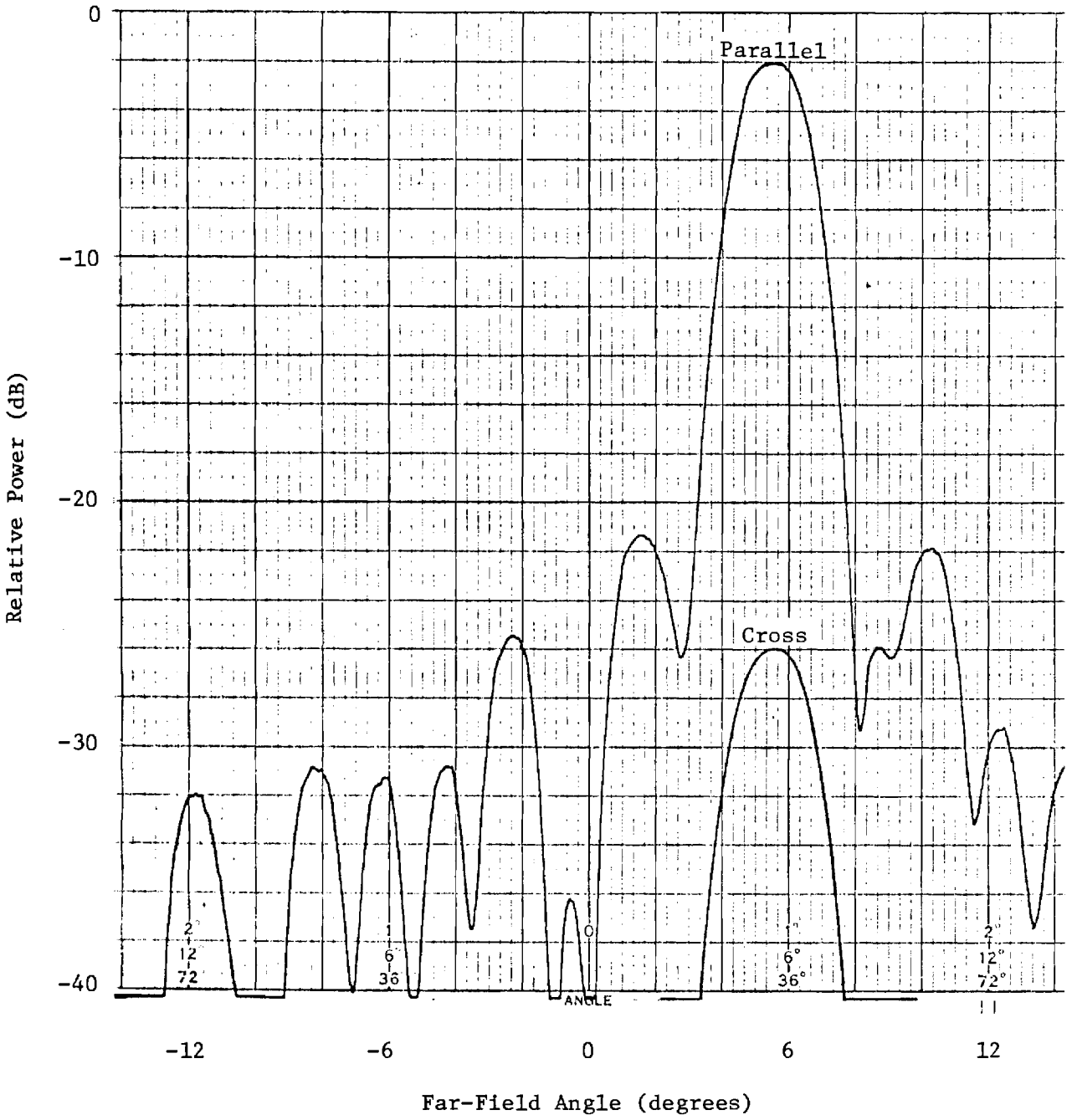

Figure 22. Far-field azimuth pattern for the edge-slot array antenna at 14.65 GHz; efficient design.

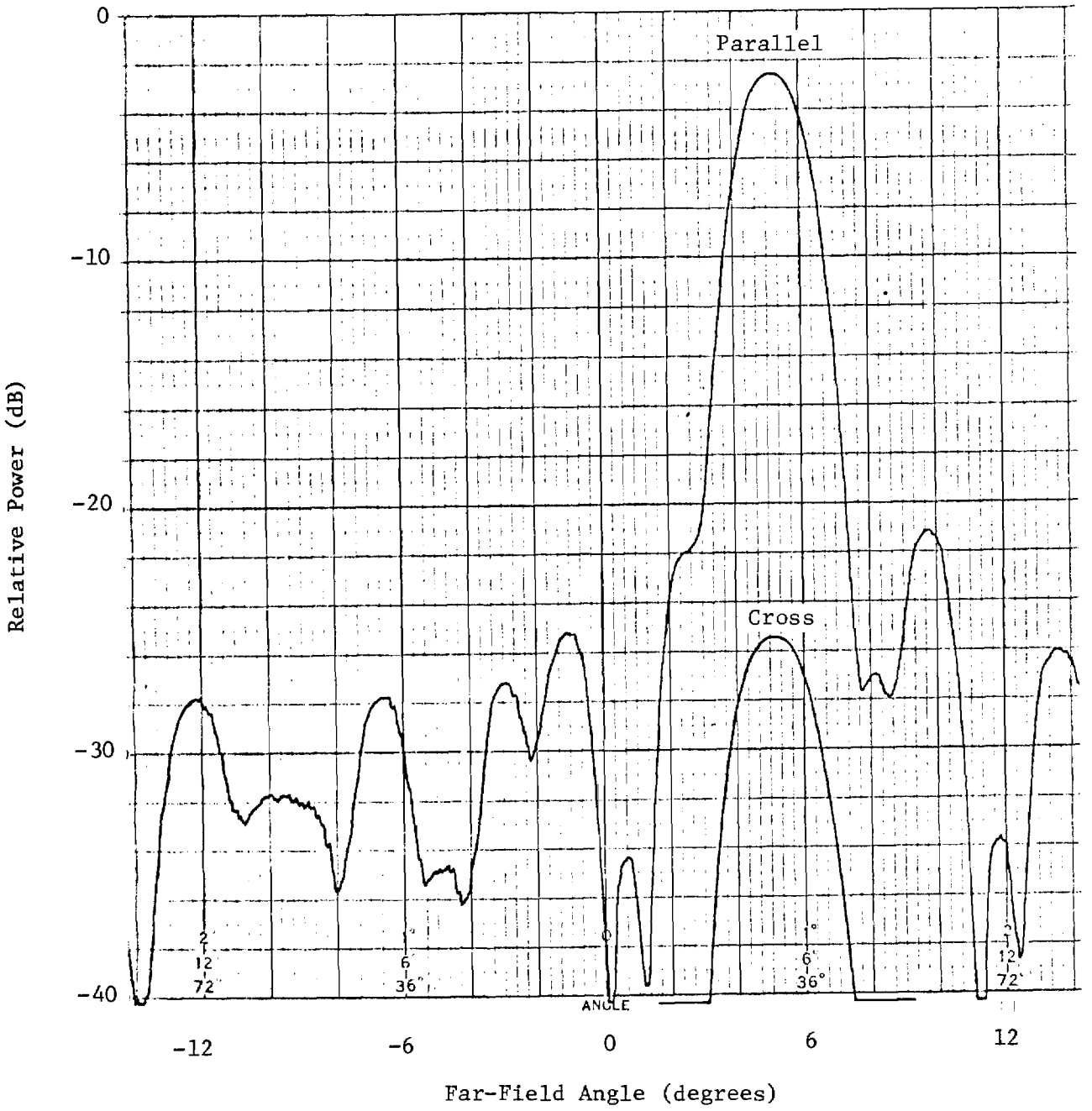

Figure 23. Far-field azimuth pattern for the edge-slot array antenna at 14.55 GHz; inefficient design.

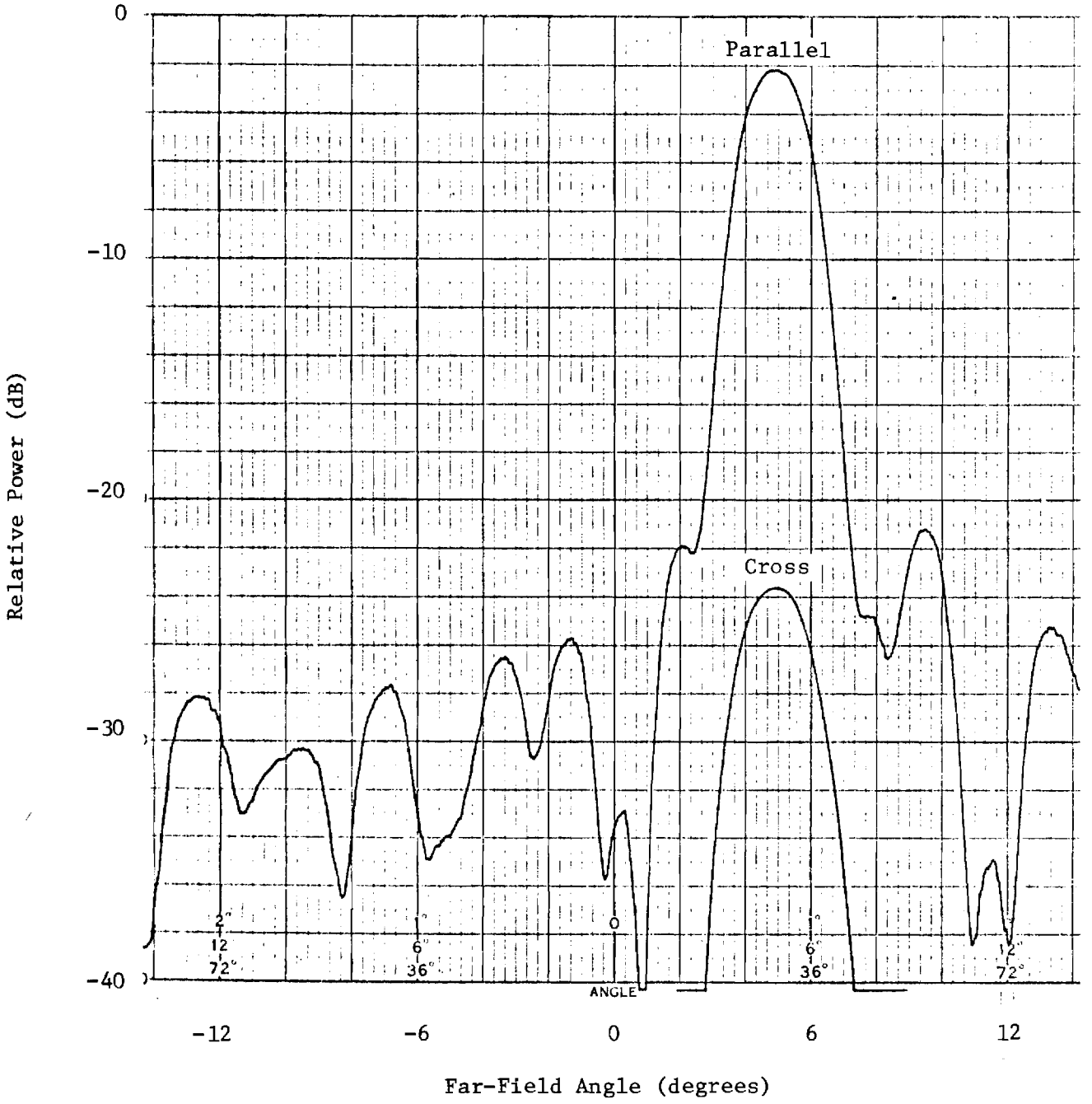

Figure 24. Far-field azimuth pattern for the edge-slot array antenna at 14.6 GHz; inefficient design.

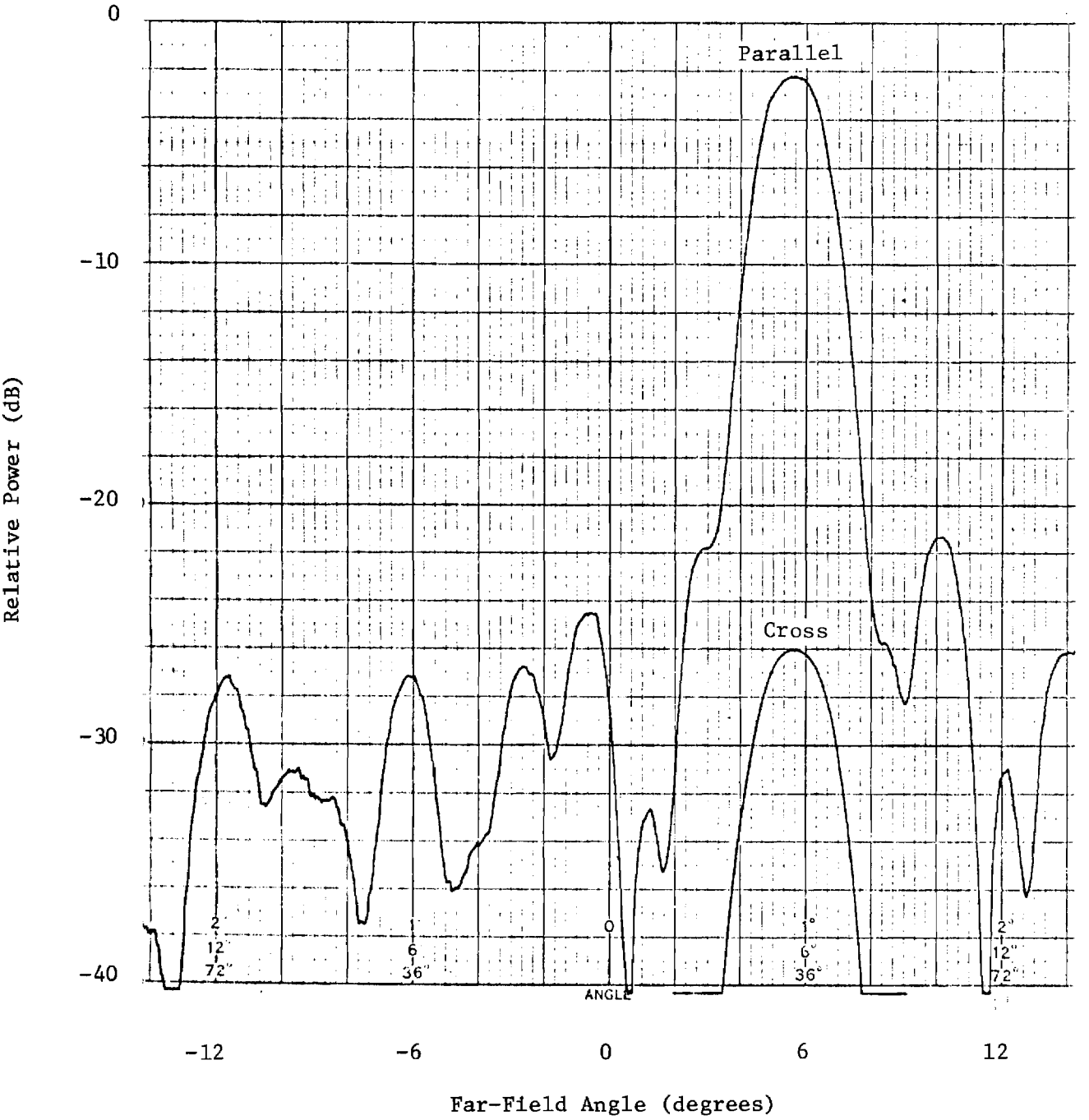

Figure 25. Far-field azimuth pattern for the edge-slot array antenna at 14.65 GHz; inefficient design.

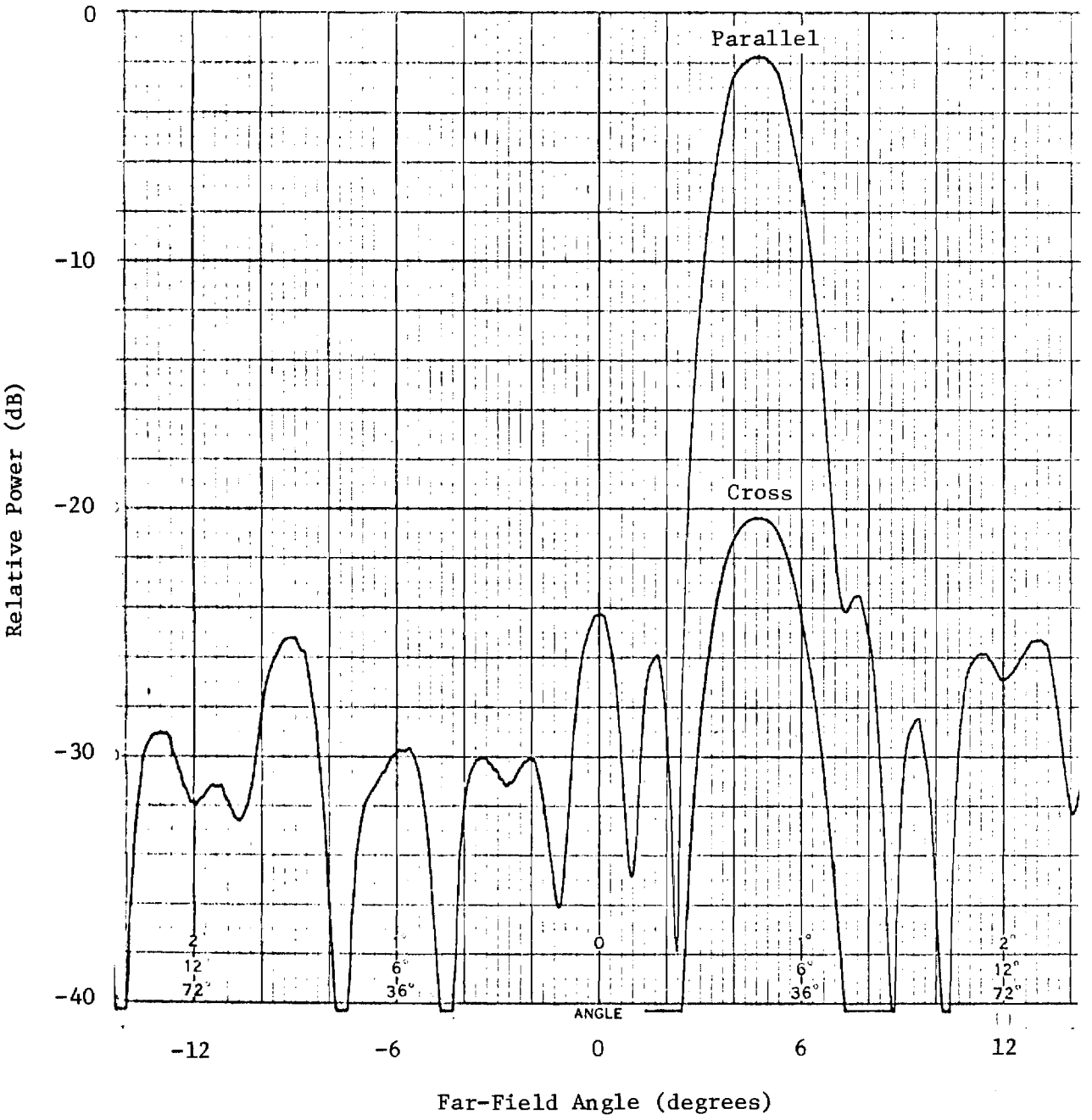

Figure 26. Far-field azimuth pattern for the broadwall-slot array antenna at 14.55 GHz; efficient design.

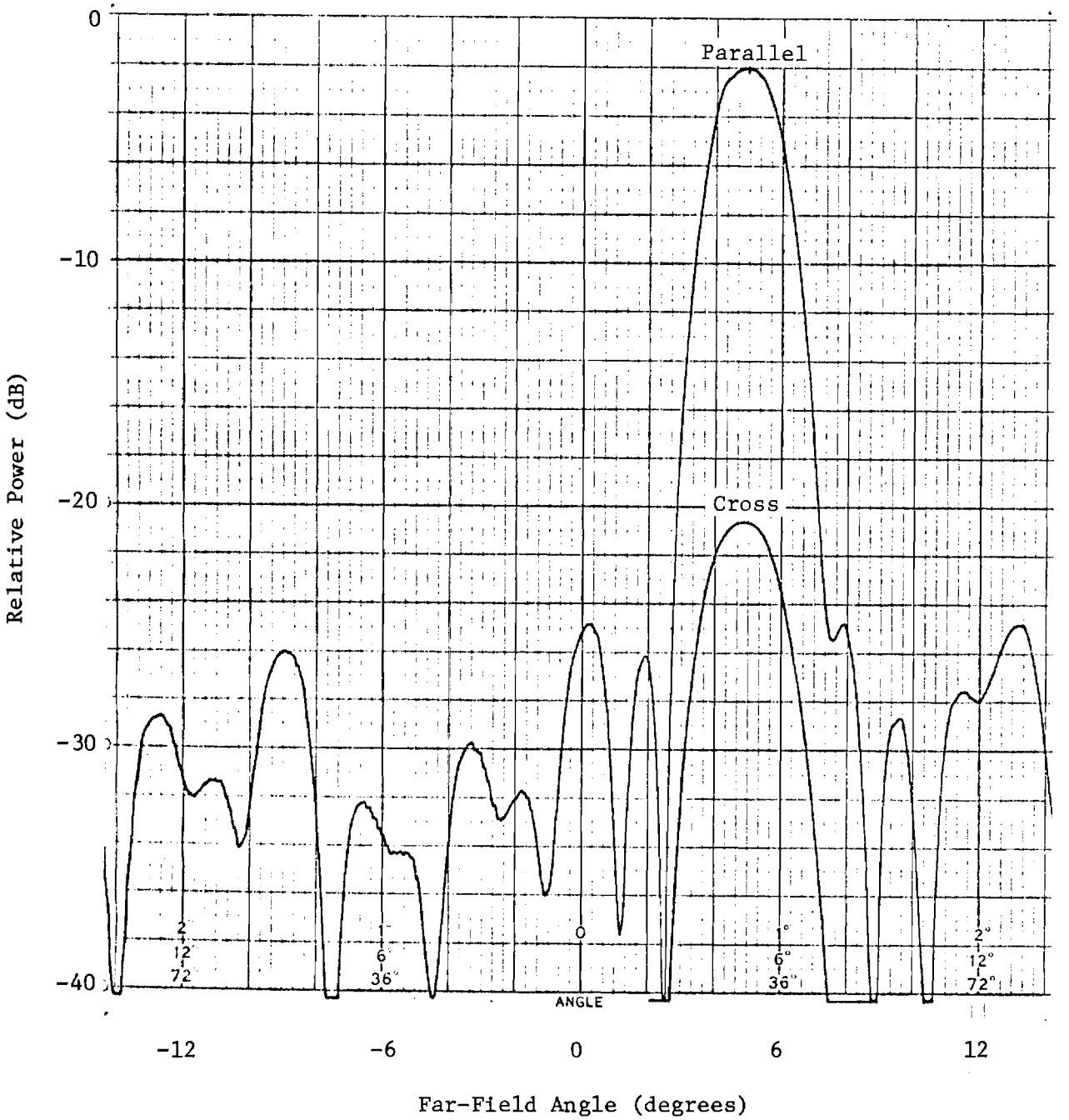

Figure 27. Far-field azimuth pattern for the broadwall-slot array antenna at 14.60 GHz; efficient design.

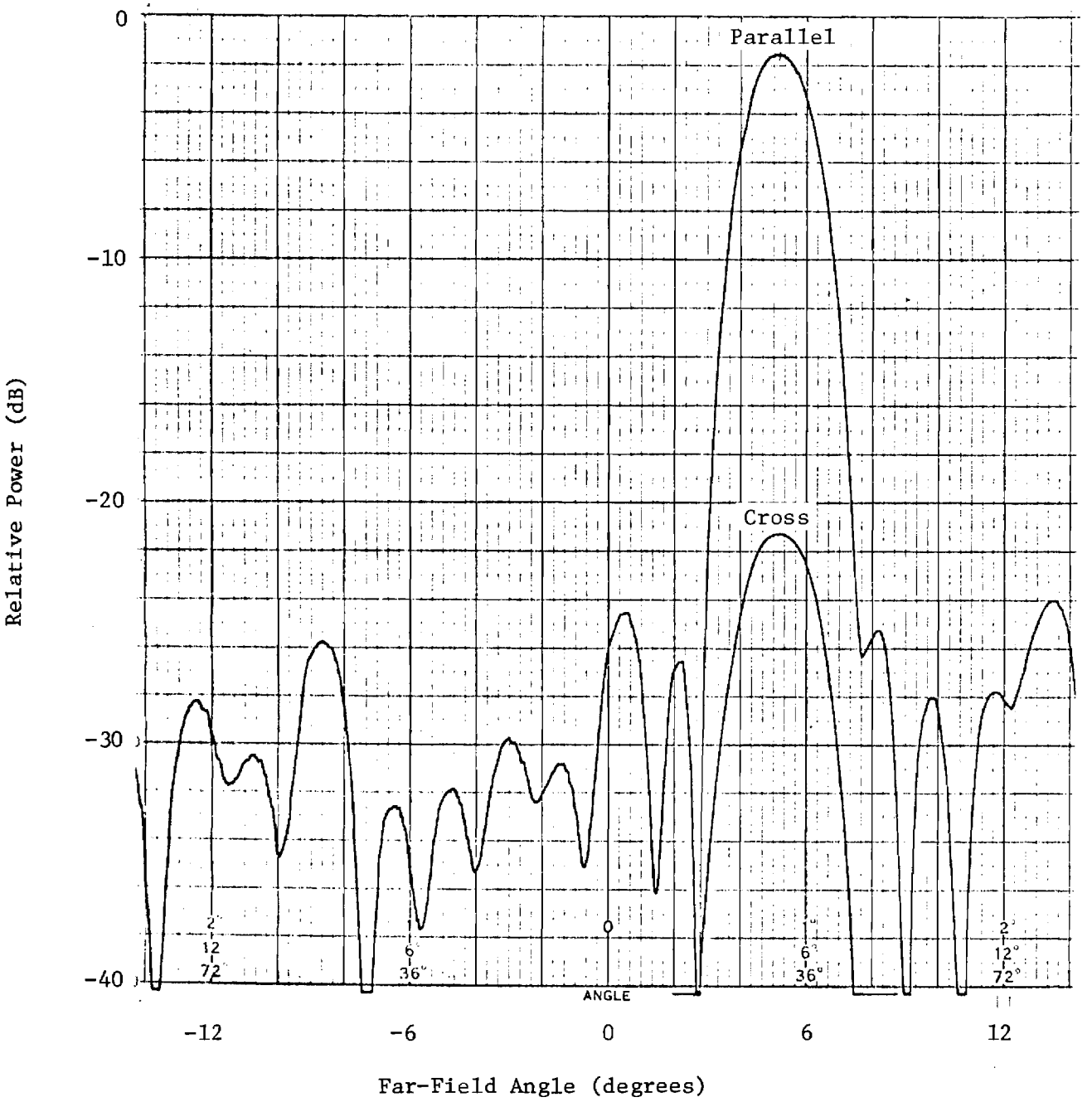

Figure 28. Far-field azimuth pattern for the broadwall-slot array antenna at 14.65 GHz; efficient design.

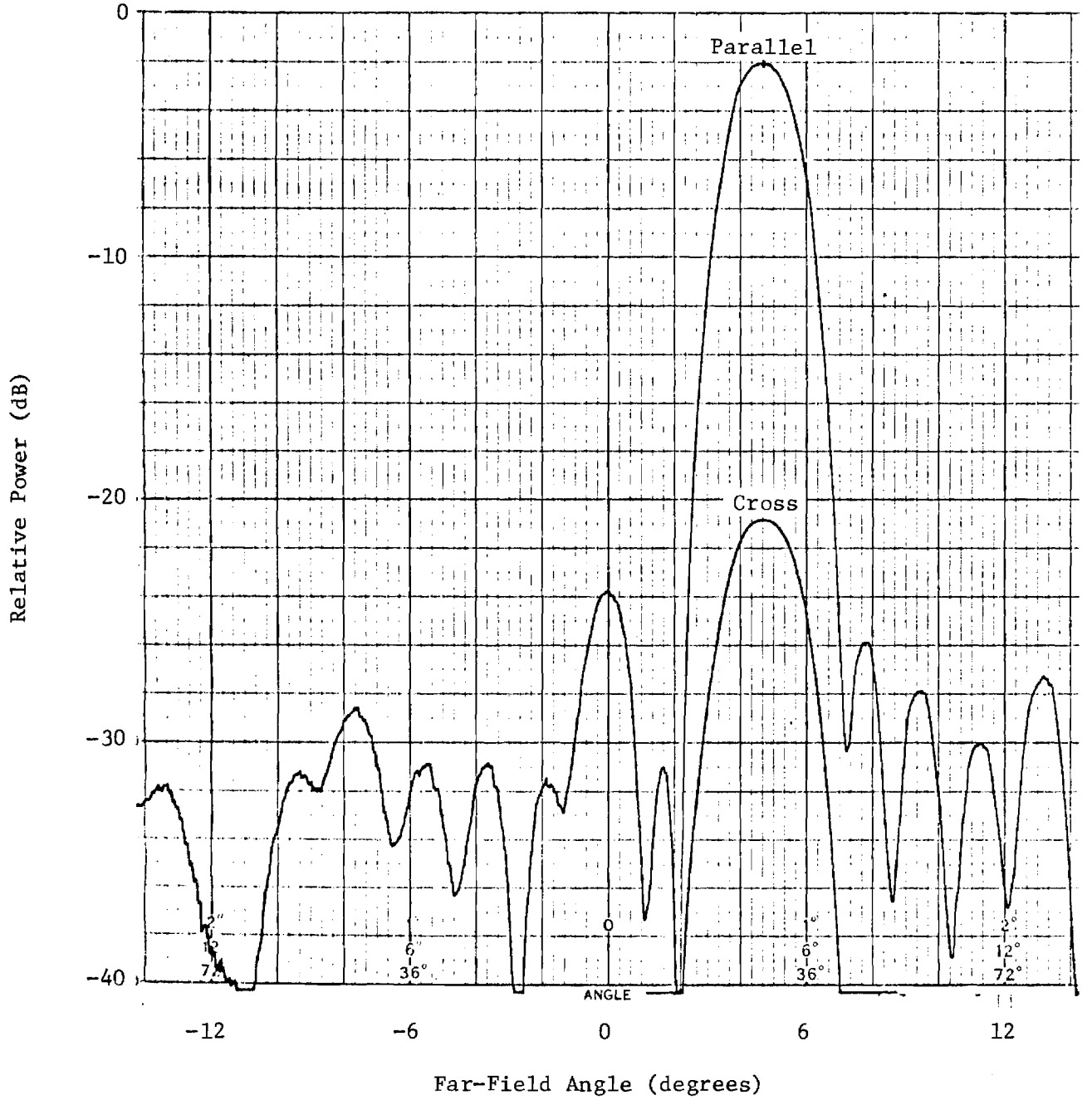

Figure 29. Far-field azimuth pattern for the broadwall-slot array antenna at 14.55 GHz; inefficient design.

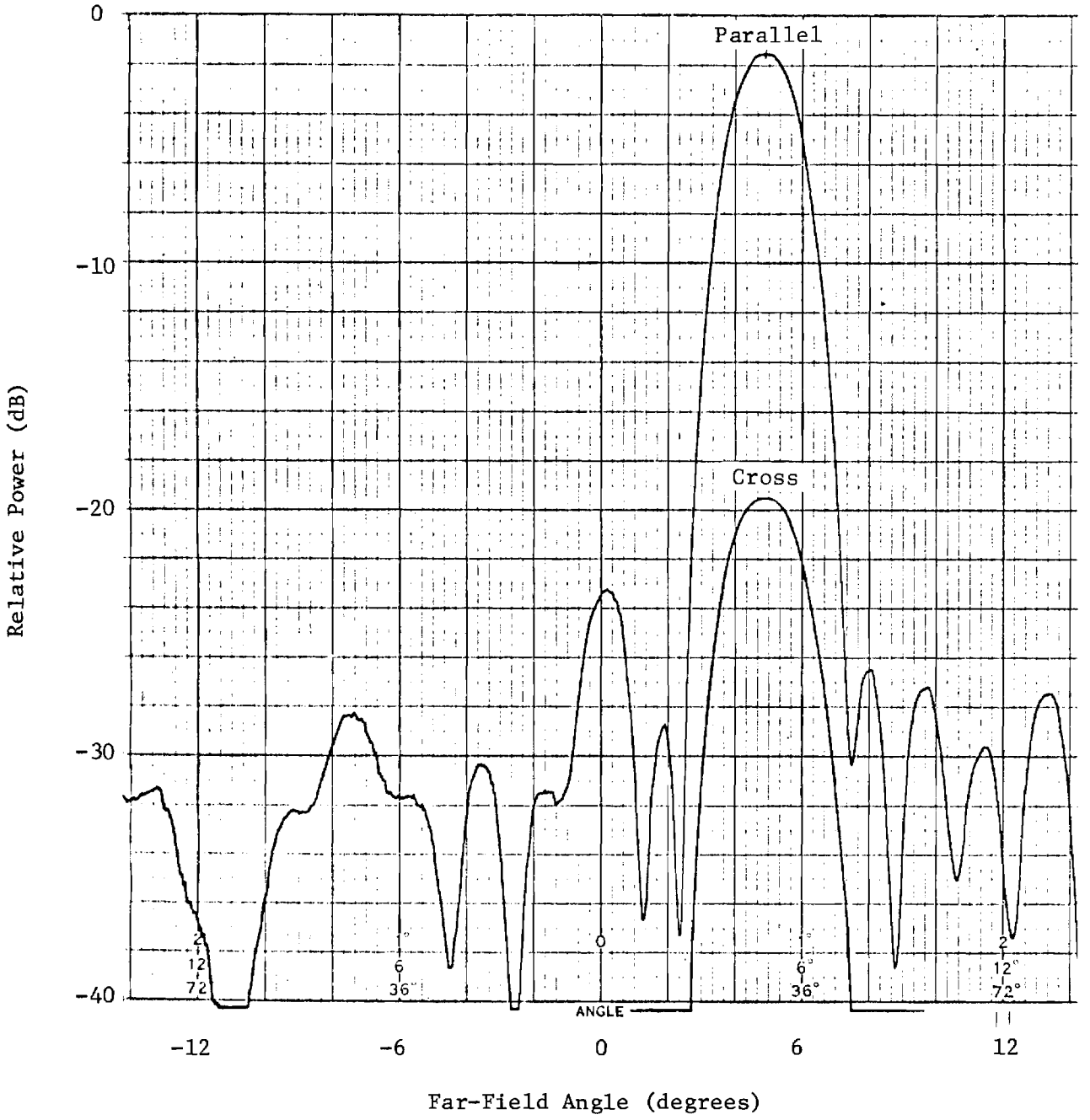

Figure 30. Far-field azimuth pattern for the broadwall-slot array antenna at 14.60 GHz; inefficient design.

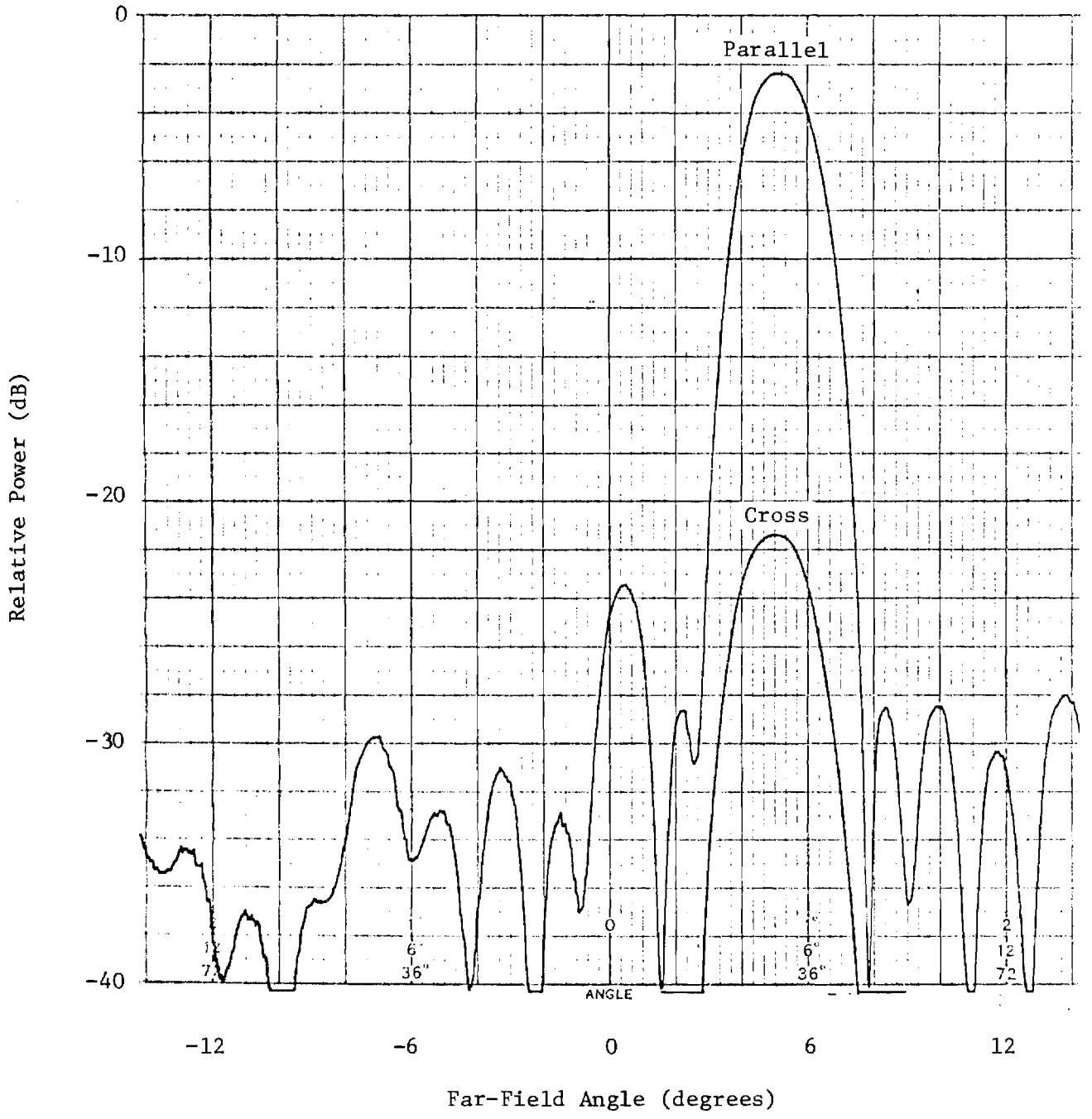

Figure 31. Far-field azimuth pattern for the broadwall-slot array antenna at 14.65 GHz; inefficient design.

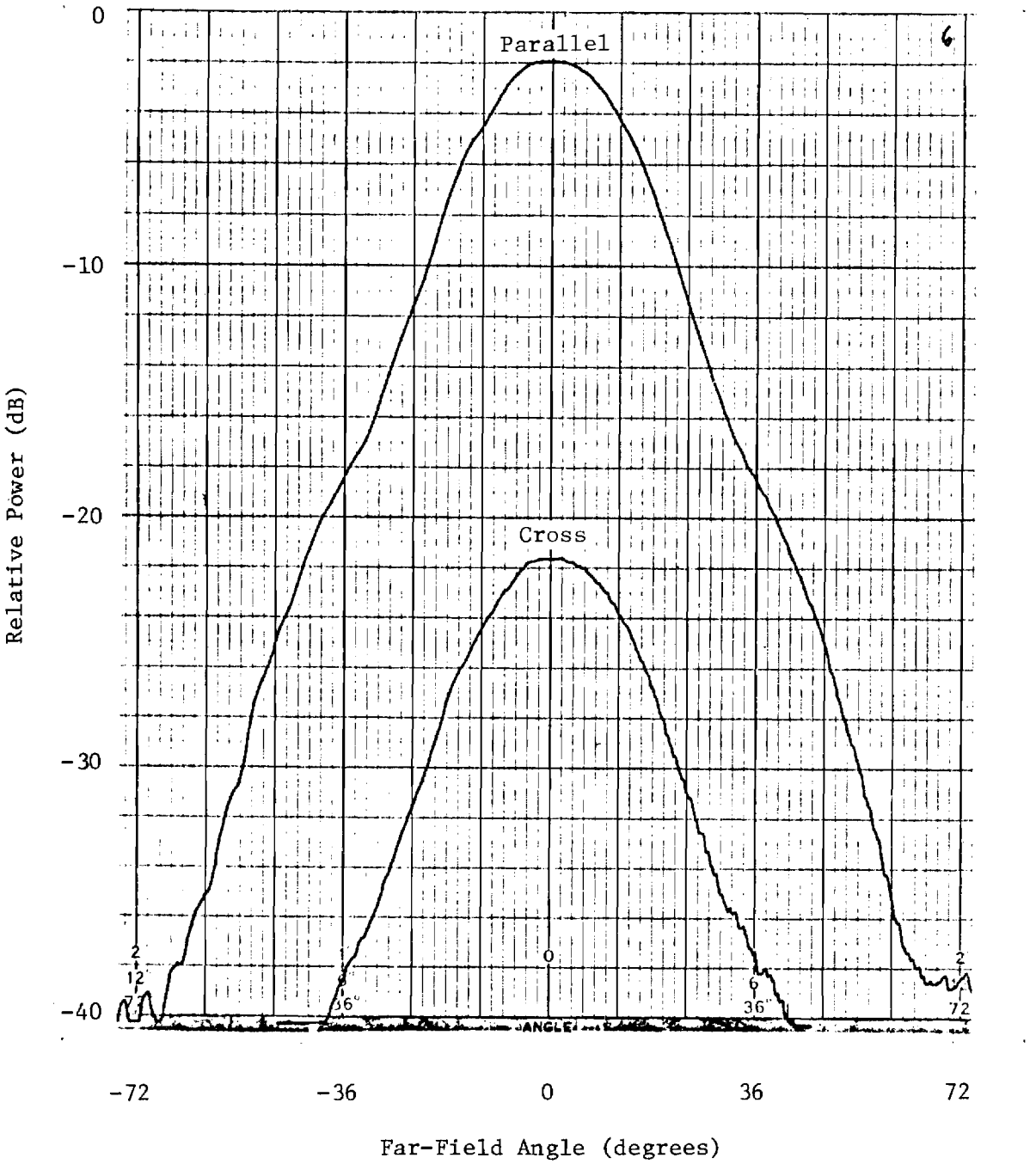

Figure 32. Far-field elevation pattern for the edge-slot array antenna at 14.55 GHz; efficient design.

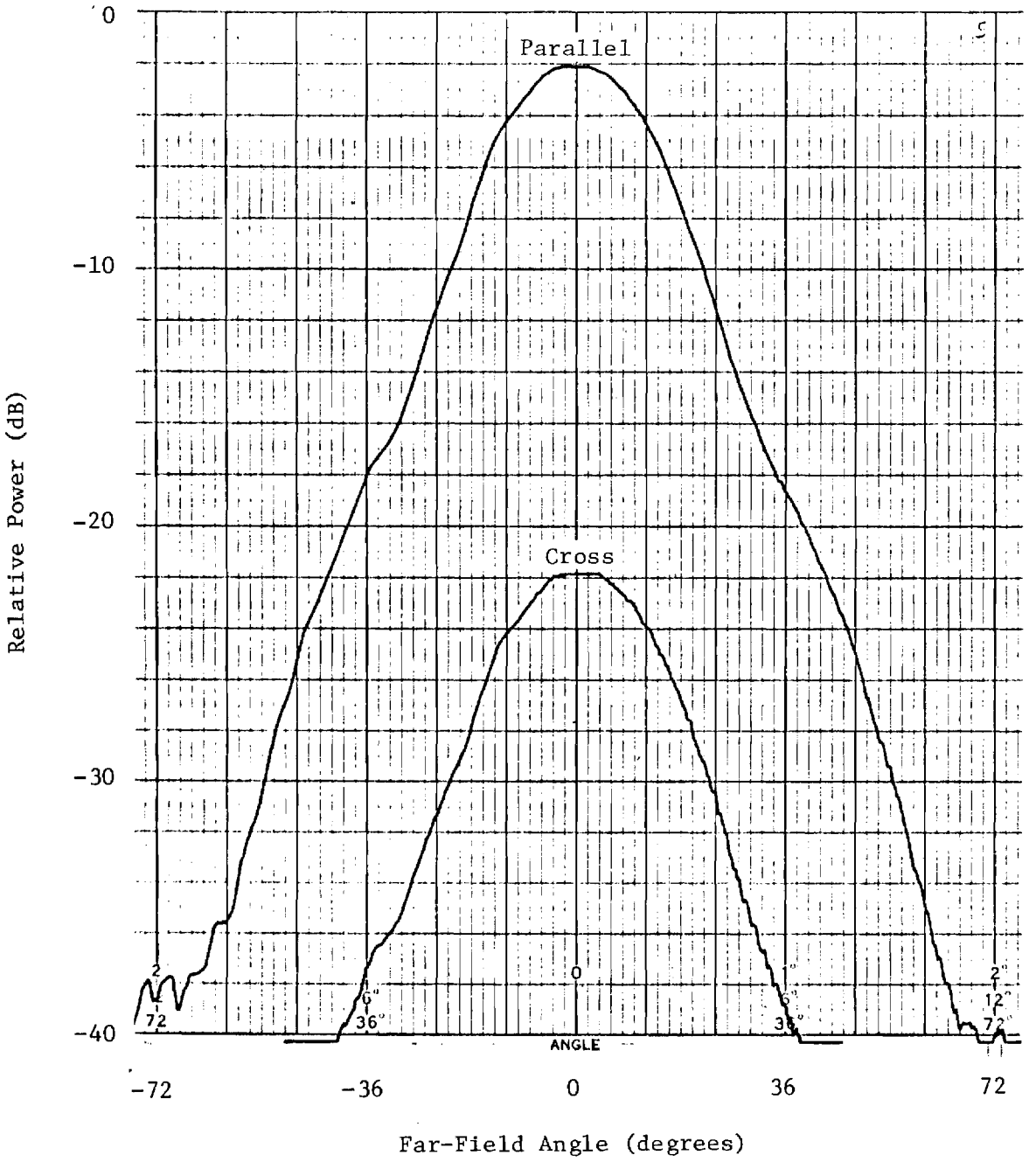

Figure 33. Far-field elevation pattern for the edge-slot array antenna at 14.60 GHz; efficient design.

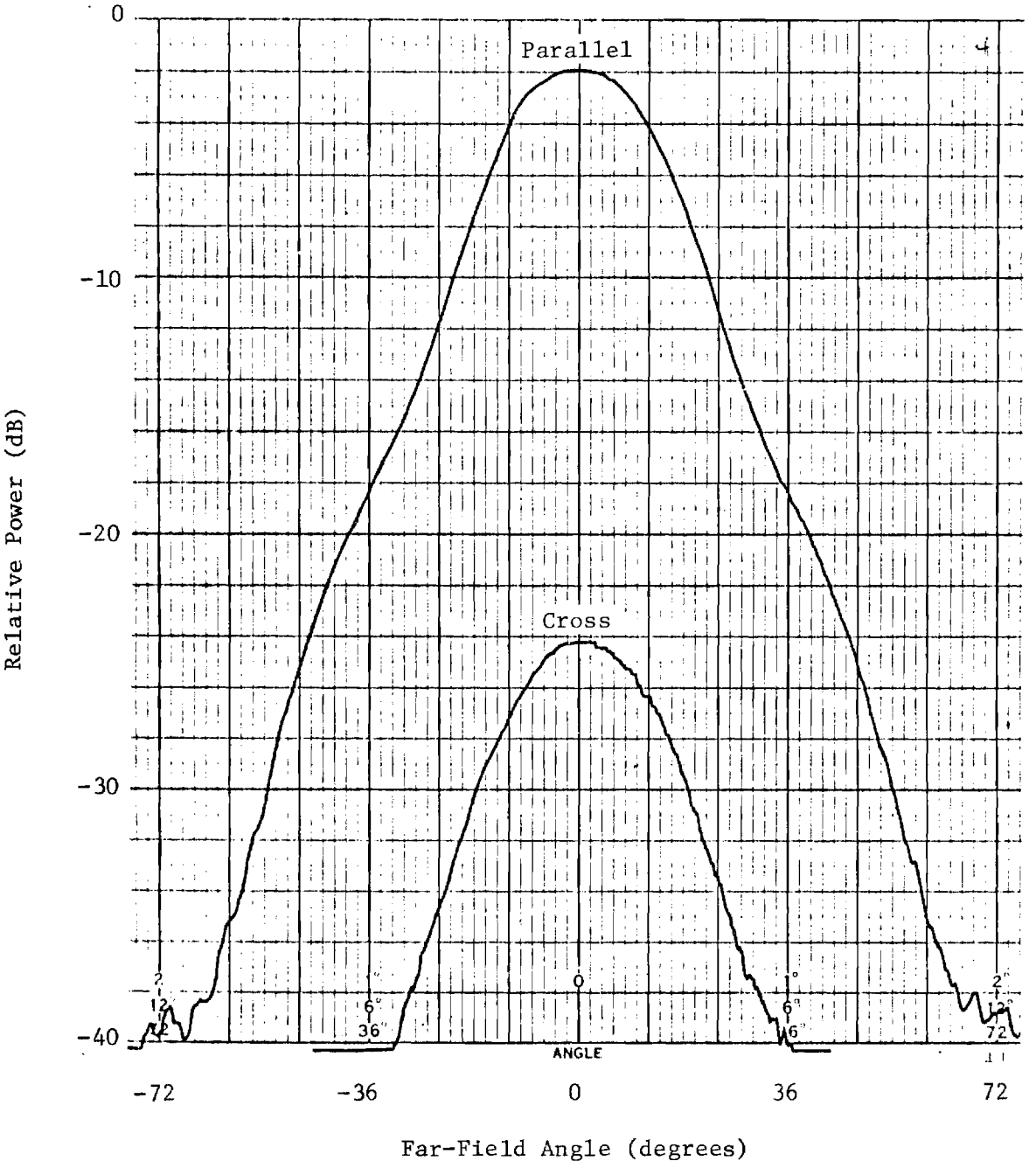

Figure 34. Far-field elevation pattern for the edge-slot array antenna at 14.65 GHz; efficient design.

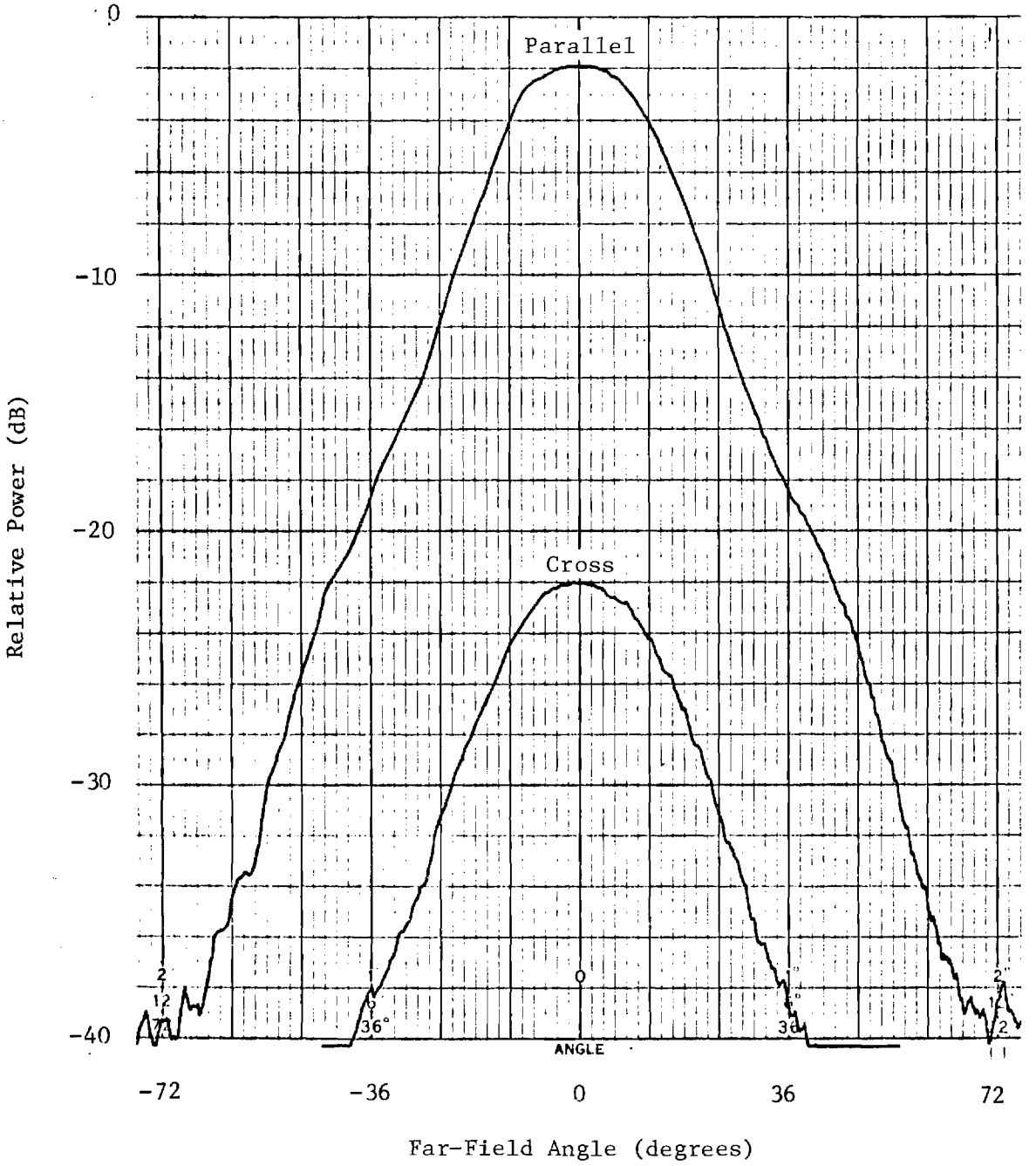

Figure 35. Far-field elevation pattern for the edge-slot array antenna at 14.55 GHz; inefficient design.

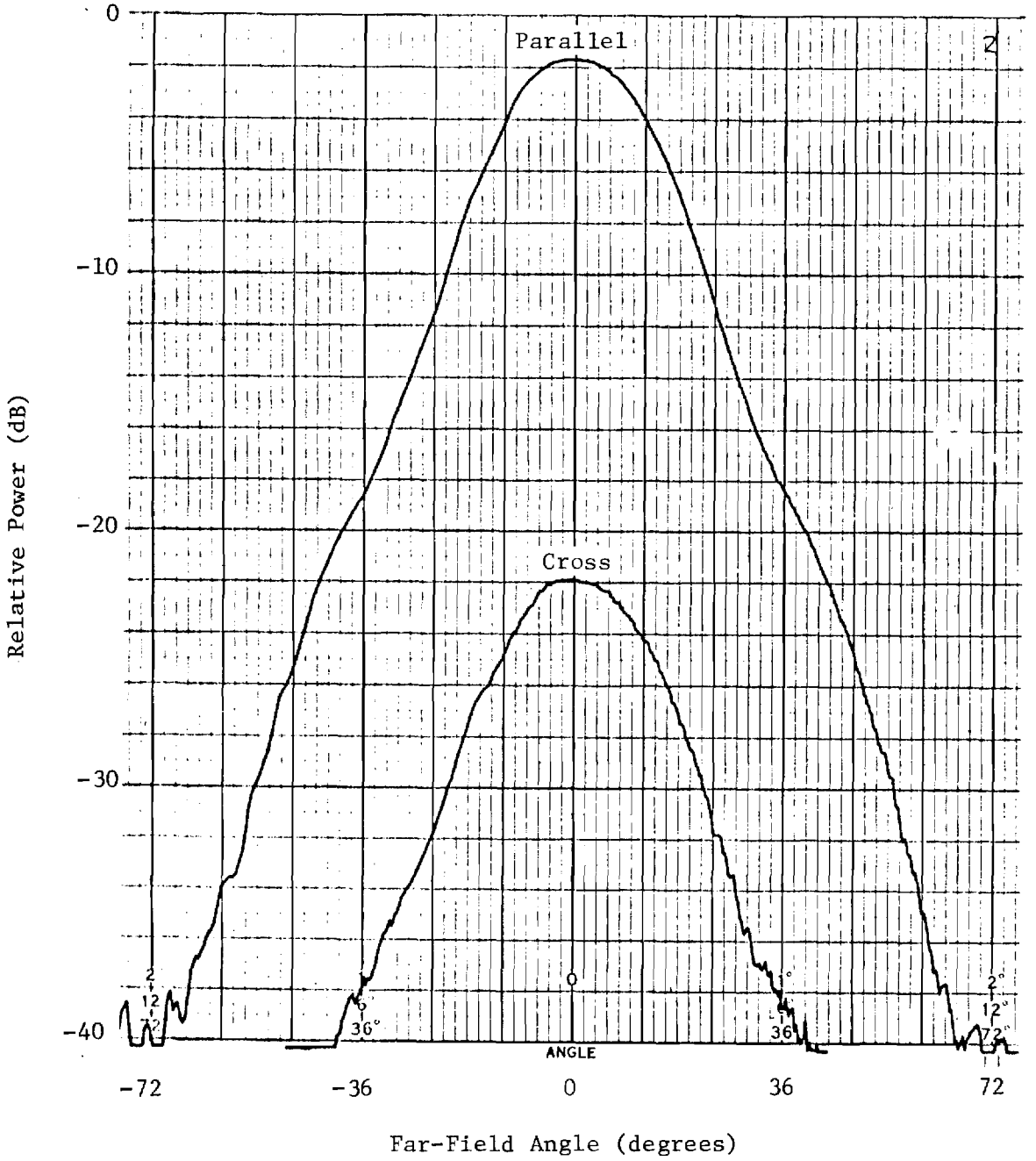

Figure 36. Far-field elevation pattern for the edge-slot array antenna at 14.6 GHz; inefficient design.

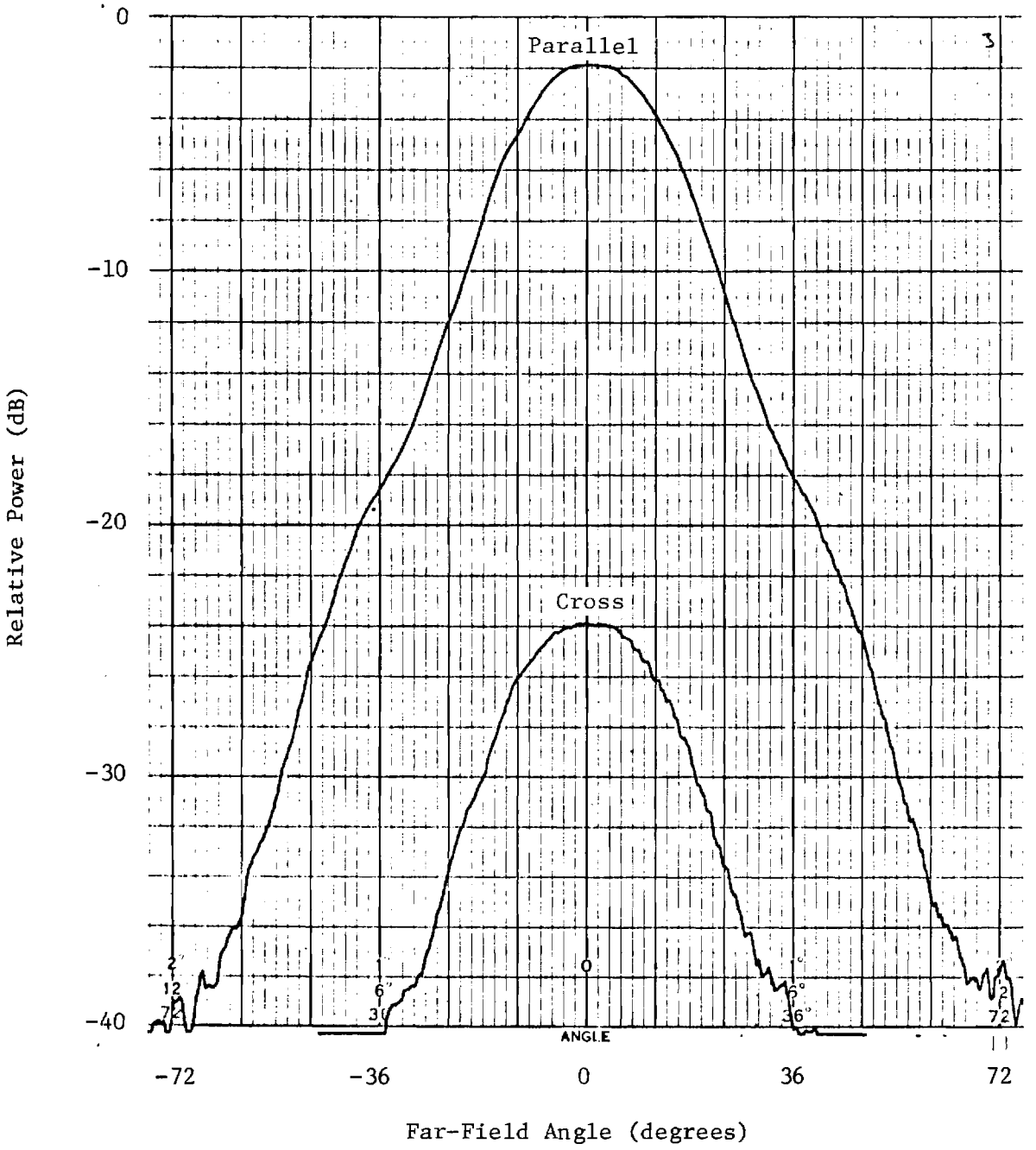

Figure 37. Far-field elevation pattern for the edge-slot array antenna at 14.65 GHz; inefficient design.

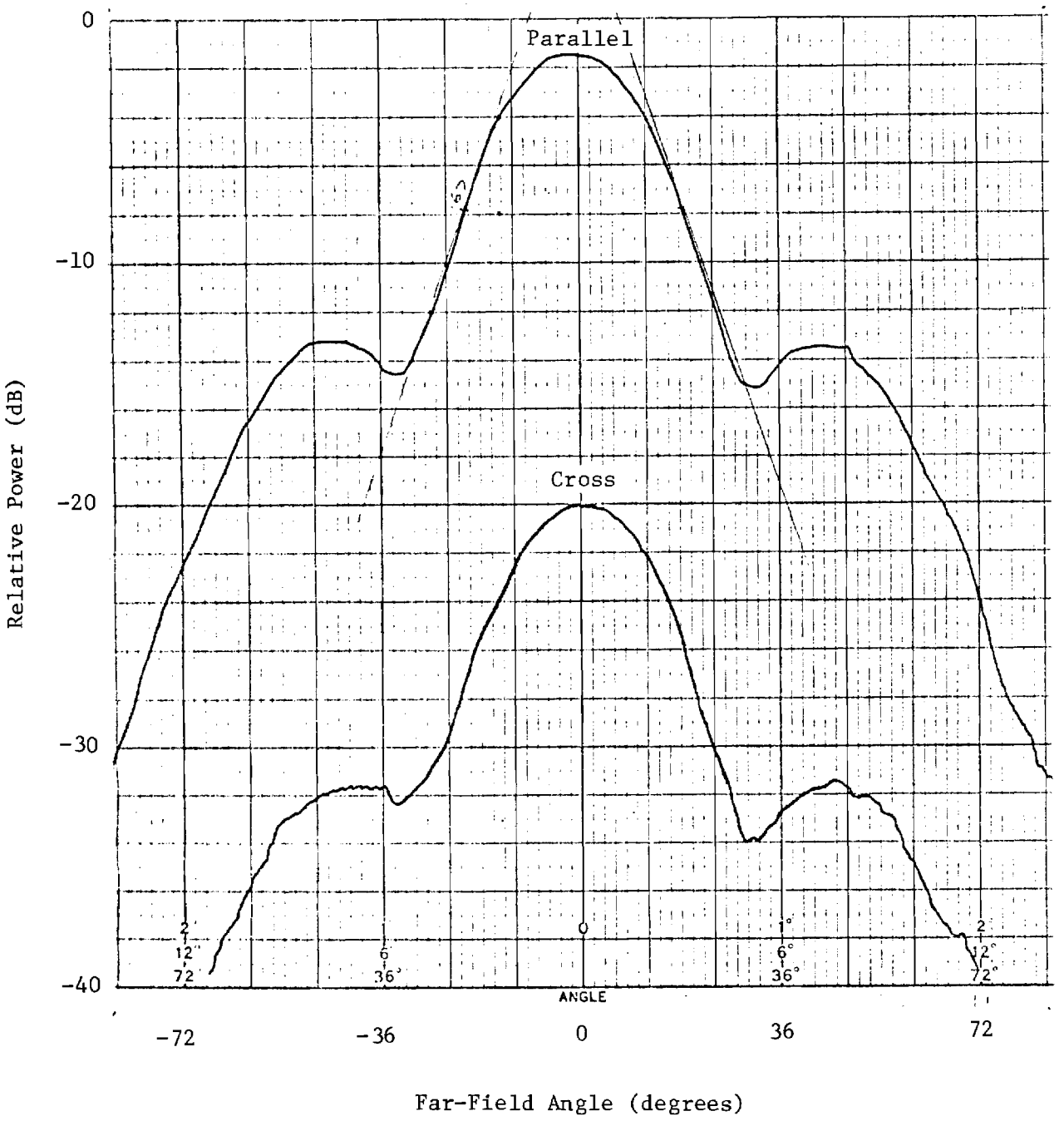

Figure 38. Far-field elevation pattern for the broadwall-slot array antenna at 14.55 GHz; efficient design.

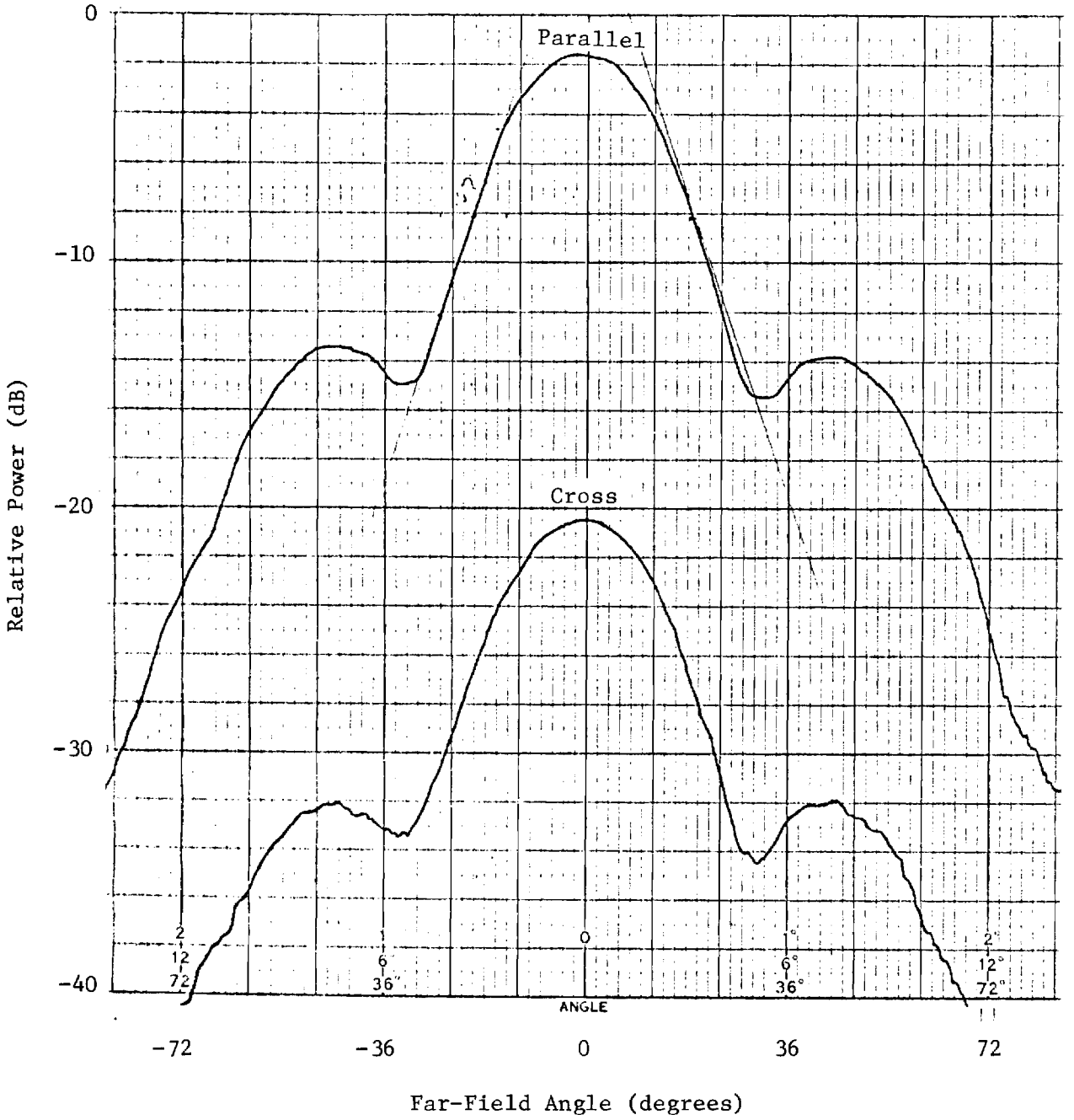

Figure 39. Far-field elevation pattern for the broadwall-slot array antenna at 14.60 GHz; efficient design.

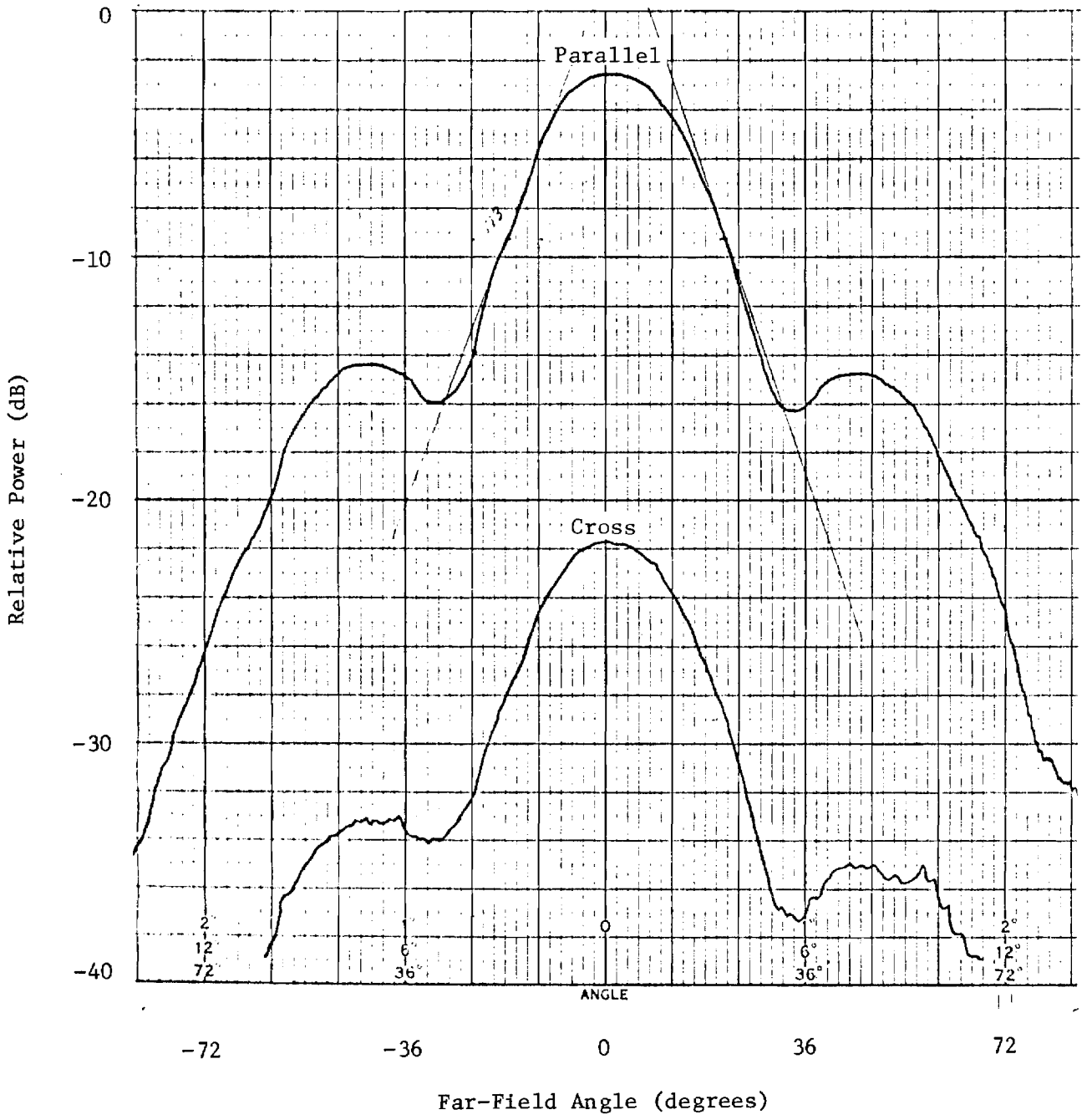

Figure 40. Far-field elevation pattern for the broadwall-slot array antenna at 14.65 GHz; efficient design.

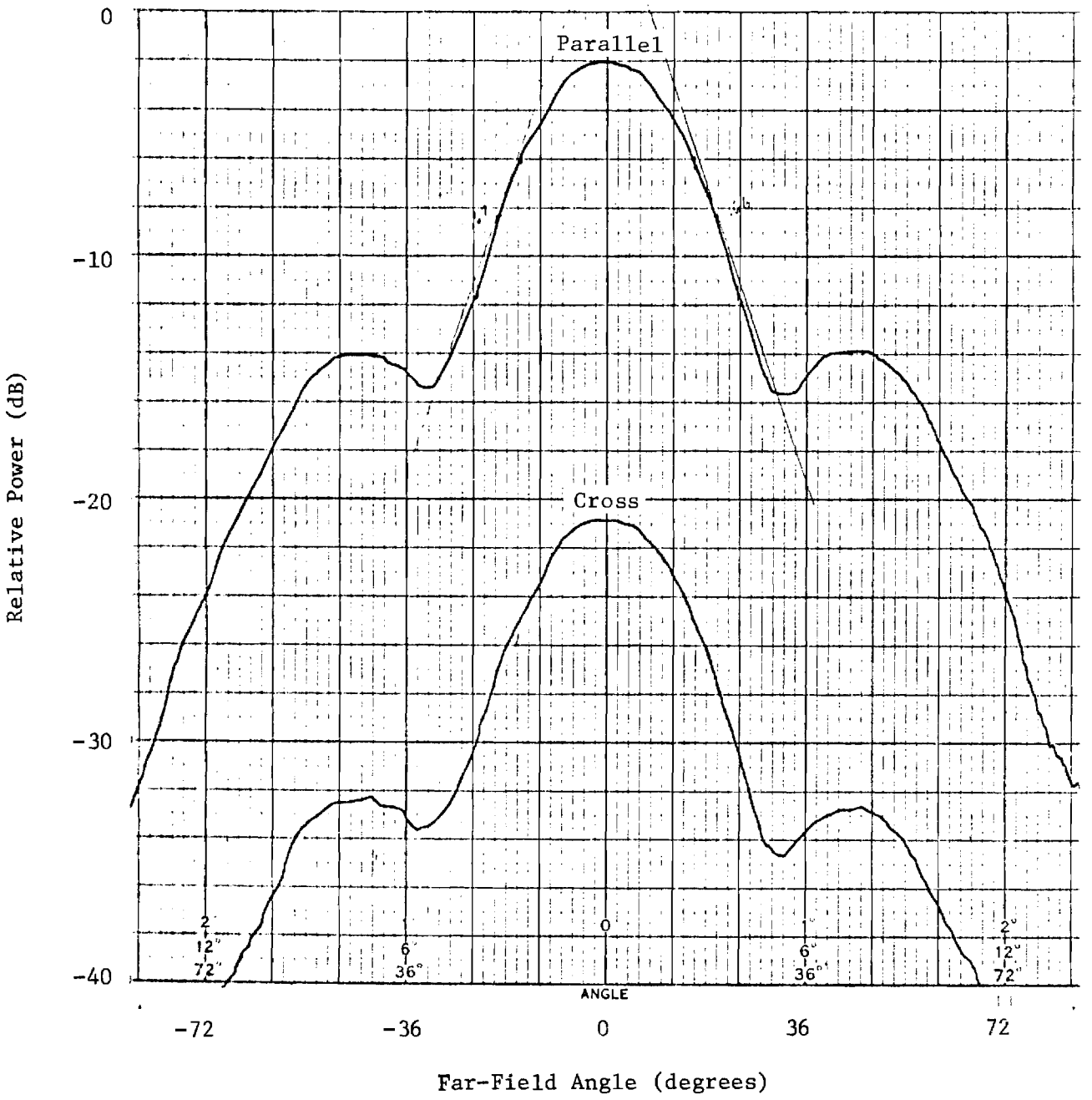

Figure 41. Far-field elevation pattern for the broadwall-slot array antenna at 14.55 GHz; inefficient design.

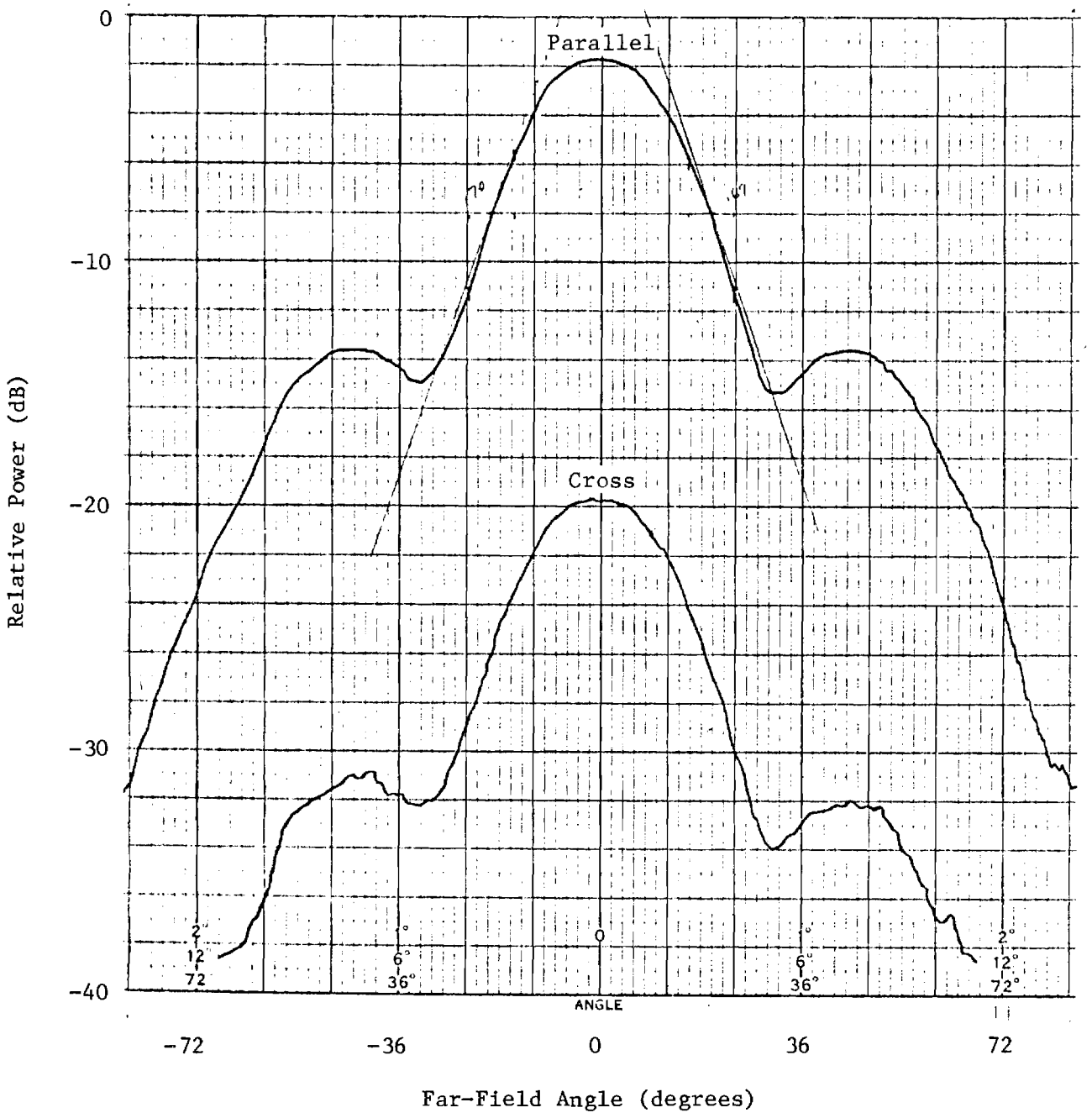

Figure 42. Far-field elevation pattern for the broadwall-slot array antenna at 14.60 GHz; inefficient design.

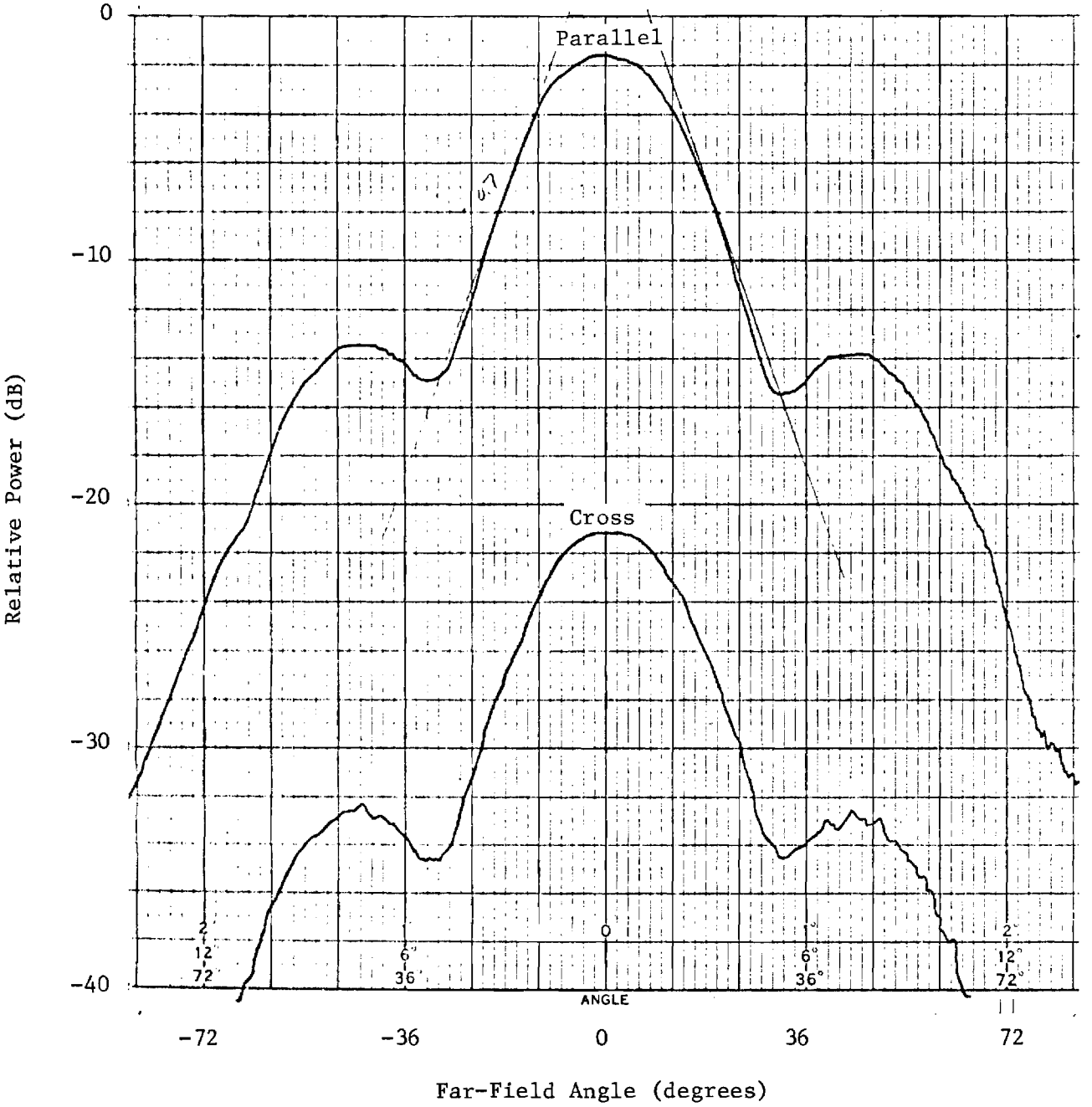

Figure 43. Far-field elevation pattern for the broadwall-slot array antenna at 14.65 GHz; inefficient design.

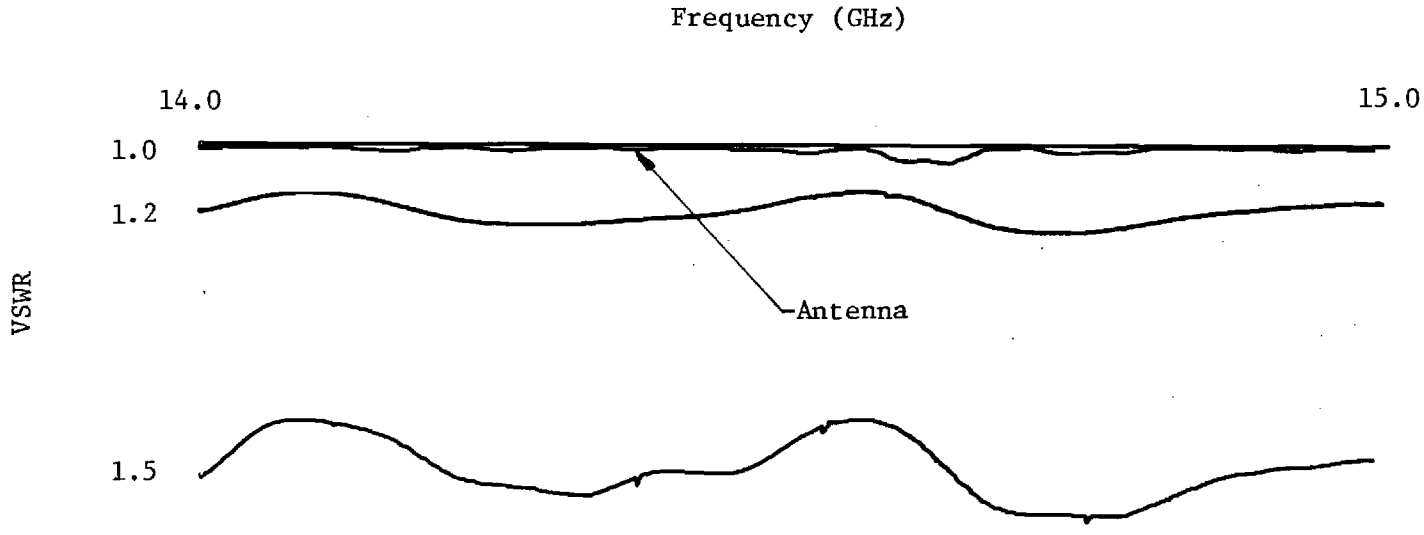

Figure 44. Swept VSWR for the broadwall-slot array antenna; efficient design; no radome.

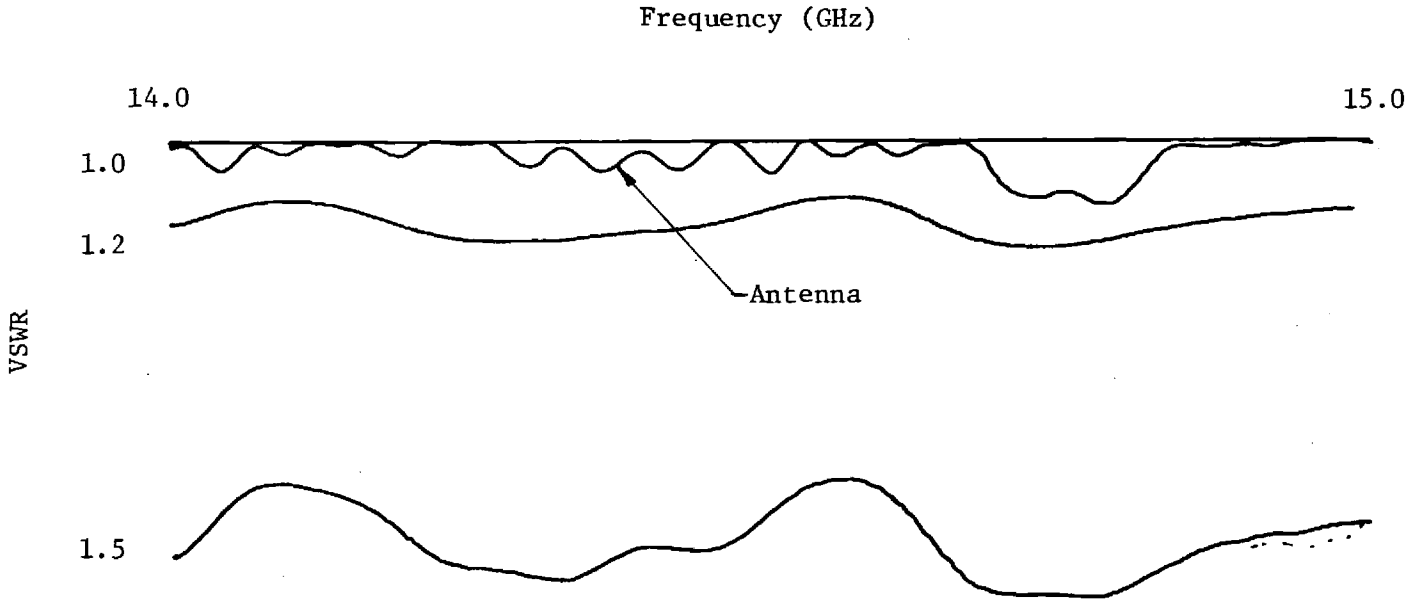

Figure 45. Swept VSWR for the edge-slot array antenna; efficient design; with thin fiberglass radome.

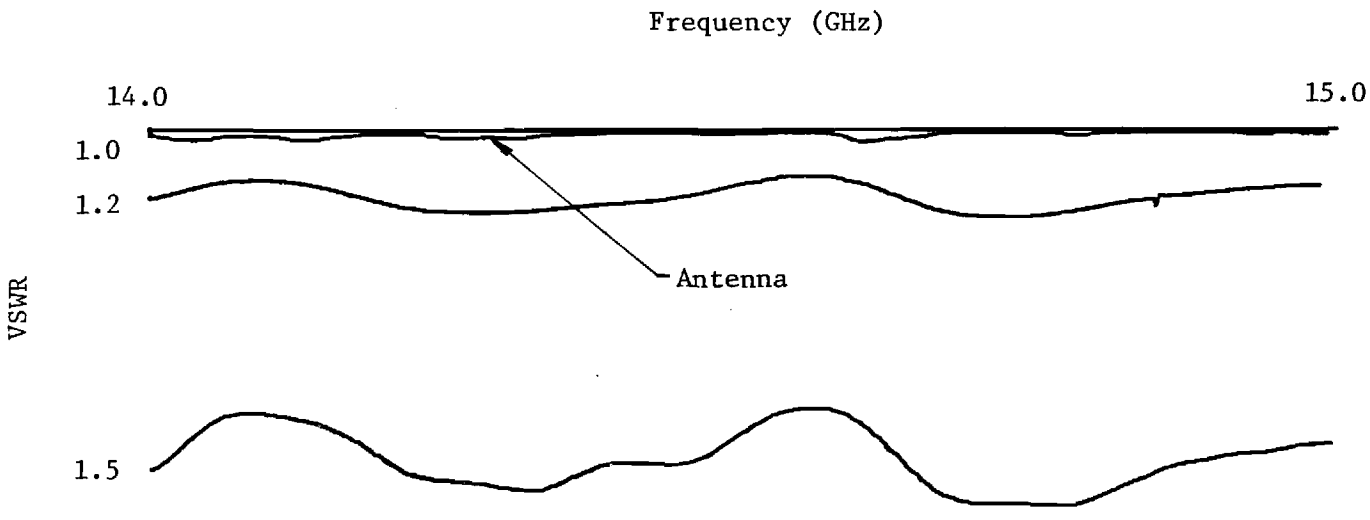

Figure 46. Swept VSWR for the edge-slot array antenna; inefficient design; no radome.

IV. CONCLUSIONS AND RECOMMENDATIONS

This report presents the preliminary SEASAT-A scatterometer antenna design performed by the Engineering Experiment Station at the Georgia Institute of Technology for the Applied Physics Laboratory. The design recommended and pursued under this study consists of a pair of slotted waveguides in separate but mechanically connected trough horns. Horizontal polarization is obtained from an edge slot waveguide array feeding one trough horn while vertical polarization is obtained from a broadwall slot array feeding a separate trough horn. A stiffened thin-wall box-beam structure is used to mechanically hold the structure to the required tolerances. Polystyrene foam insulation encapsulates the antennas, and this foam, combined with external paint coatings, provides temperature control for the antenna.

The proposed design uses proven techniques for achieving the electrical and mechanical performance specified in Tables I and II of this report. Electrical, mechanical, and thermal analyses indicated that the proposed antenna concept can provide the desired electrical and mechanical performance. Quarter length, full frequency models of the proposed antennas were built and tested. Test results indicate that the desired electrical performance can be achieved using the proposed design.

V. REFERENCES

1. D. G. Bodnar, "SEASAT Antenna Study," Final Technical Report, Project A-1617-000, APL/JHU Subcontract 600128, Task 1 under Prime Contract N00017-72-C-4401, Engineering Experiment Station, Georgia Institute of Technology, August 1974.

2. G. A. Deschamps, "Determination of Reflection Coefficients and Insertion Loss of a Wave-Guide Junction," Journal of Applied Physics, August 1953, pp. 1046-1050.

3. Handbook of Tables for Applied Engineering Science, Ray E. Bolz and George L. Tuve, Ed., The Chemical Rubber Co., Cleveland, Ohio, 1970.

4. John B. Rittenhouse and John B. Singletary, Space Materials Handbook, Third Edition, NASA, SP-3051, Washington, D.C., 1969.

5. "Computer Program for Determining the Thermal Environment and Temperature History of Earth Orbiting Space Vehicles," The Boeing Co., Document No. D5-13284, NASA MFS-12879, COSMIC, Athens, Georgia, August, 1966.

6. J. D. Gaski, L. C. Fink, and T. Ishimoto, Systems Improved Numerical Differencing Analyzer Users Manual, TRW Systems, NASA MSC-13805, COSMIC, Athens, Georgia, September 1970.

Unclassified

SECURITY CLASSIFICATION OF THIS PAGE *(When Data Entered)*

REPORT DOCUMENTATION PAGE		READ INSTRUCTIONS BEFORE COMPLETING FORM
1. REPORT NUMBER EES/GIT Project A-1617-010	2. GOVT ACCESSION NO.	3. RECIPIENT'S CATALOG NUMBER
4. TITLE *(and Subtitle)* Preliminary SEASAT-A Scatterometer Antenna Design		5. TYPE OF REPORT & PERIOD COVERED Final Technical Report 6. PERFORMING ORG. REPORT NUMBER
7. AUTHOR*(s)* D. G. Bodnar, N. T. Alexander, and R. R. Sheppard		8. CONTRACT OR GRANT NUMBER*(s)* Prime Contract N00017-72-C-4401 and APL/JHU Subcontract 600128, Task 5
9. PERFORMING ORGANIZATION NAME AND ADDRESS Engineering Experiment Station Georgia Institute of Technology Atlanta, Georgia 30332		10. PROGRAM ELEMENT, PROJECT, TASK AREA & WORK UNIT NUMBERS
11. CONTROLLING OFFICE NAME AND ADDRESS Naval Ordnance Systems Command Washington, D.C. 20360		12. REPORT DATE October 1975 13. NUMBER OF PAGES 78 + vii
14. MONITORING AGENCY NAME & ADDRESS*(if different from Controlling Office)* Applied Physics Laboratory The Johns Hopkins University 8621 Georgia Avenue Silver Spring, Maryland 20910		15. SECURITY CLASS. *(of this report)* Unclassified 15a. DECLASSIFICATION/DOWNGRADING SCHEDULE
16. DISTRIBUTION STATEMENT *(of this Report)*		
17. DISTRIBUTION STATEMENT *(of the abstract entered in Block 20, if different from Report)*		
18. SUPPLEMENTARY NOTES		
19. KEY WORDS *(Continue on reverse side if necessary and identify by block number)* Antennas, arrays, waveguide antennas, thermal design		

20. ABSTRACT *(Continue on reverse side if necessary and identify by block number)*

A preliminary electrical, mechanical, and thermal design for the Mode I and Mode II flight antennas of the SEASAT-A satellite scatterometer has been performed. A non-resonant edge-slot array in a trough horn provides horizontal polarization, and a separate non-resonant broadwall slot array in a similar trough horn provides vertical polarization. These antennas operate at 14.6 GHz and combine to produce a dual polarized fan beam. A stiffened thin-wall box-beam structure is used to maintain the requisite mechanical tolerances. Both

(continued)

DD FORM 1 JAN 73 1473 EDITION OF 1 NOV 65 IS OBSOLETE

Unclassified

SECURITY CLASSIFICATION OF THIS PAGE *(When Data Entered)*

20. Abstract (continued)

mechanical and electrical design considerations of the antenna are presented. Full frequency, quarter-length brassband model antennas were fabricated for both the edge slot and broadwall slot arrays and tested for conformance to the current specifications. Measured data on these antennas is presented and indicates that the desired performance from the full length antennas can be achieved with the design utilized.